Interpolating vector fields for near identity maps and averaging

V. Gelfreich[1] and A. Vieiro[2]

[1] Mathematics Institute, University of Warwick, Coventry CV4 7AL, UK

v.gelfreich@warwick.ac.uk

[2] Departament de Matemàtiques i Informàtica,

Universitat de Barcelona, Gran Via 585, 08007 Barcelona, Spain

vieiro@maia.ub.es

May 3, 2018

Abstract

For a smooth near identity map, we introduce the notion of an interpolating vector field written in terms of iterates of the map. Our construction is based on Lagrangian interpolation and provides an explicit expressions for autonomous vector fields which approximately interpolate the map. We study properties of the interpolating vector fields and explore their applications to the study of dynamics. In particular, we construct adiabatic invariants for symplectic near identity maps. We also introduce the notion of a Poincaré section for a near identity map and use it to visualise dynamics of four dimensional maps. We illustrate our theory with several examples, including the Chirikov standard map, a volume-preserving map and a symplectic map in dimension four. The last example is motivated by the theory of Arnold diffusion.

1 Introduction

Near identity maps naturally appear in several branches of mathematics and mathematical physics. They are often used for numerical integration of ordinary differential equations and for studying the evolution under fast time-periodic forcing. In the perturbation theory of integrable Hamiltonian systems with three degrees of freedom, near identity maps are used to describe dynamics in a small neighbourhood of a double resonance, see e.g. [8]. The last problem is one of the central topics in the study of the Arnold diffusion. In these problems some important details of the discussion depend on the smoothness class of the map and, for the sake of simplicity, we mainly consider the infinitely differentiable case and, where appropriate, assume analyticity.

It is well known that a near identity map F_ϵ, where $|\epsilon| \ll 1$ and $F_0 = \mathrm{I}$, is formally embedded into an autonomous flow [16]. Indeed, a formal construction can be used to find a vector field in the form of a formal power series in ϵ such that the formal series of the corresponding time-ϵ map coincides with the Taylor series of the original map. Truncated series define a vector field which interpolates the map with an error of order of the first omitted term. Note that this construction is formal only as in general the map cannot be embedded into an autonomous flow, i.e. generic F_ϵ cannot be represented as a time-ϵ map of an autonomous vector field [10]. Nevertheless, the difference between them can be made a flat function in ϵ at $\epsilon = 0$ [14]. In the analytic case, the difference becomes exponentially small in ϵ when the series are optimally truncated [1].

An alternative approach to the study of near identity maps is based on averaging (see e.g. [10]). A near identity map F_ϵ can be written as a time-ϵ map of a time-periodic vector field called a *suspension* of the map. Then the averaging procedure can be used recursively to eliminate the time-dependence up to any order of the small parameter. In the analytic case, a suspension can be found in the form of an analytic autonomous vector field plus an exponentially small non-autonomous term [10] (see also [3] for a concrete example). In order to make the paper more self-contained, we sketch the construction of a suspension and averaging procedure in Section 2.3. The corresponding arguments are based on the implicit function theorem and involve vectorfields which are analytic in the space variables but only C^∞ in time. We note that a suspension can be made analytic both in the space variables and time [9] but the corresponding construction is more complicated, moreover, the analyticity in time is not essential for the application of the averaging theory.

Both these methods are constructive, nevertheless, none of them provides an easy way to find an explicit expression for a vector field which approximately interpolates the map. In this paper we propose a new method for construction of such vector fields henceforth referred to as *interpolating vector fields*. The interpolating vector fields are represented in the form of weighted sums of iterates of the map, i.e. $\epsilon X_n = \sum_{k=-n}^{n} p_{nk} F_\epsilon^k$. Therefore our construction can be considered as a discrete version of the averaging method. The weights p_{nk} are constants determined explicitly with the help of the Lagrange interpolation.

The simplicity of the expressions for the interpolating vector fields turn them into a useful tool for analysis of dynamics. In particular, we introduce the notion of a "Poincaré section" for the map F_ϵ. Similarly to classical Poincaré section, this construction reduces the dimension of the phase space by one and, consequently, can be used to visualise trajectories of four-dimensional maps. We note that the method of slices can be used to achieve the same goal (see e.g. [12]). Of course, the method of slices is applicable to a wider class of maps as it does not require the map to be near identity. On other hand, if the map is near identity, the interpolating vector fields have a potential for refining the method of slices by taking into account the dynamics: orthogonal projections used in the method of slices may be replaced by projections along an interpolating vector field in hope of getting a better representation of invariant sets using a smaller number of iterates. A more detailed comparison of the methods can be found in Section 3.3.

In the case when the map F_ϵ is symplectic, an interpolating vector field X_n can be used

to construct an adiabatic invariant h_n. The function h_n is approximately preserved for many iterates of the map and can be used for a further reduction of the dimension.

In order to illustrate the effectiveness of the method and before discussing technical details involved in the construction, let us consider a 4-dimensional near identity Froeschlé-like symplectic diffeomorphism T_ϵ defined on $\mathbb{T}^2 \times \mathbb{R}^2$. In coordinates $(\psi_1, \psi_2, J_1, J_2)$ this map is defined by the equation (3.6) but the precise expression is not important for the current discussion. Let Σ be a three-dimensional cylinder defined by the equality $\psi_1 = \psi_2$. Fig. 1(a) shows points from several trajectories of T_ϵ projected along an interpolating vector field onto Σ. We call this picture *a Poincaré section for the map* T_ϵ.

In Fig. 1 all initial conditions are chosen from a torus defined by the intersection of Σ with a level set of the adiabatic invariant h_{10}. Since h_{10} is approximately preserved by the map, all points shown on Fig. 1(a) are in a small neighbourhood of the torus. Then a clearer image of the dynamics is obtained with the help two angular coordinates, namely, ψ and $\phi = \arg(J_1 + iJ_2)$. Fig. 1(b) shows the projection of Fig. 1(a) onto the torus (ψ_1, ϕ), and Fig. 1(c) is a magnification of a strip located near the top of Fig. 1(b). These pictures reveal that the four-dimensional dynamics of T_ϵ resemble a two-dimensional area-preserving map. This similarity can be explained with the help of the normal form theory [11]. The latter also provides an alternative visualisation method (see [6]). We stress that the method of this paper is much easier to implement and provides higher accuracy in representation of details of the dynamics as our pictures represent true trajectories of T_ϵ since the interpolation is used only for selecting initial conditions and projecting points onto Σ. The details of the model and the method are described in Section 3.

To give more formal definitions for the objects discussed in this paper, consider a smooth one-parameter near identity family of maps $F_\epsilon : D \to \mathbb{R}^m$ where $m \geq 1$, $D \subset \mathbb{R}^m$ is an open domain and $|\epsilon| < \epsilon_0$. Then the map can be written in the form

$$F_\epsilon(x) = x + \epsilon\, G_\epsilon(x)\,,$$

where G_ϵ depends smoothly on x and ϵ. The function G_0 obtained by setting $\epsilon = 0$ is often called *a limit vector field*. Its time-ϵ map is ϵ^2-close to F_ϵ.

The central object of this paper is *an interpolating vector field* for the near identity map F_ϵ defined in the following way. Fix a positive integer n. Let $x \in D$ and suppose that the iterates $x_k = F_\epsilon^k(x) \in D$ are defined for $-n \leq k \leq n$. Then there is a unique polynomial p_n of degree $2n$ in t such that

$$x_k = p_n(t_k, x_0, \epsilon) \tag{1.1}$$

for every $t_k = \epsilon k$ with $|k| \leq n$. The coefficients of p_n depend on x and ϵ. The interpolating vector field is defined as the velocity vector of the interpolating curve at $t = 0$, i.e.,

$$X_n(x, \epsilon) = \partial_t p_n(0, x, \epsilon) \tag{1.2}$$

where $\partial_t p_n$ denotes the derivative of p_n with respect to t. In Section 2 we will use the Lagrange interpolation to show that the interpolating vector field X_n is a linear combination

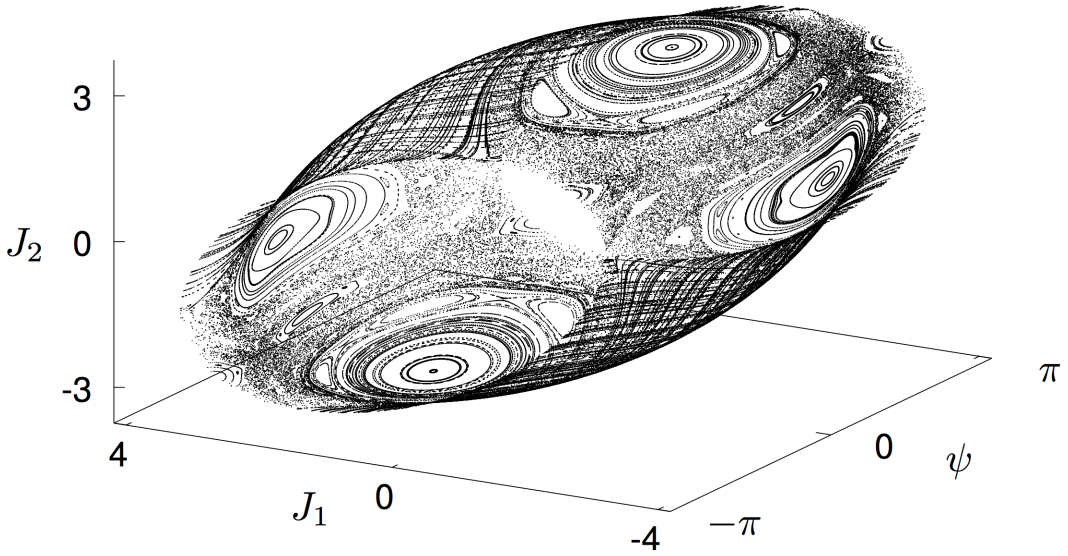

(a)

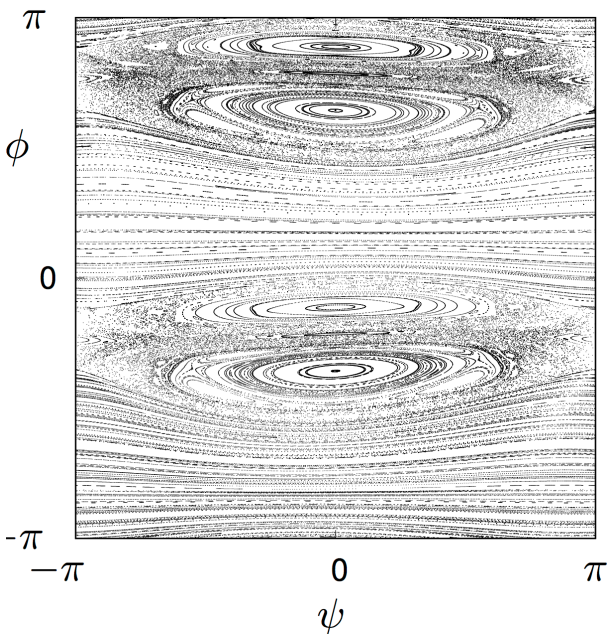

(b)

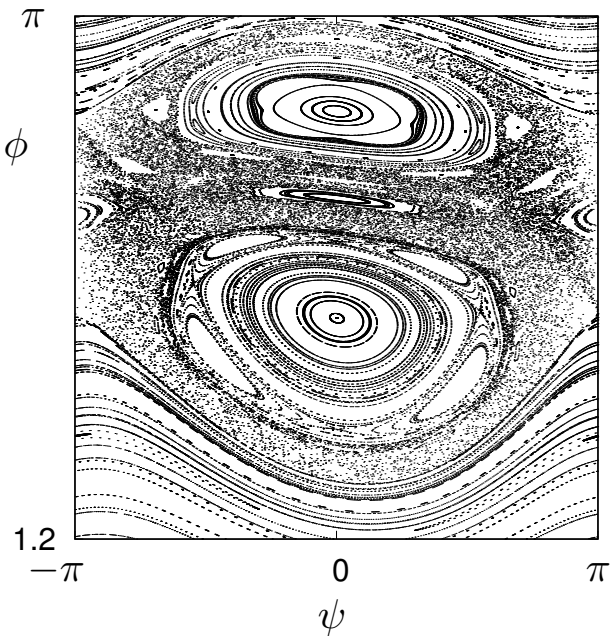

(c)

Figure 1: Dynamics of a symplectic map on a four-dimensional cylinder $\mathbb{T}^2 \times \mathbb{R}^2$. The map is defined by (3.6) with parameter given by (3.7), $\epsilon = 0.35$, and 400 initial conditions are taken on $\Sigma \cap \{h_{10} = 4\}$ (see Section 3 for details of the model and numerical techniques used to produce these pictures). (a) Trajectories of the map are projected on a three-dimensional Poincaré section (a three dimensional cylinder $\mathbb{T} \times \mathbb{R}^2$) along an interpolating vector field. Note that all points are in a small neighbourhood of a two-dimensional torus. (b) A two dimensional projection of (a) using the coordinate $\phi = \arg(J_1 + iJ_2) \in (-\pi, \pi]$ for the vertical axis. The analogy with the phase space of a two-dimensional area-preserving map is apparent. (c) A magnification of (b) where further details can be observed.

of the iterates of the initial point $x = x_0$,

$$X_n(x,\epsilon) = \epsilon^{-1} \sum_{k=1}^{n} p_{nk} \left(x_k - x_{-k}\right), \tag{1.3}$$

where

$$p_{nk} = \frac{(-1)^{k+1}(n!)^2}{k(n+k)!(n-k)!}. \tag{1.4}$$

Note that the coefficients p_{nk} are independent of the map F_ϵ. In particular, for $n = 1$ we get

$$X_1(x,\epsilon) = \frac{F_\epsilon(x) - F_\epsilon^{-1}(x)}{2\epsilon}.$$

The time-ϵ map of this vector field is ϵ^3-close to F_ϵ. Thus the flow of X_1 provides more accurate interpolation for F_ϵ than the limit flow.

Let $\Phi^t_{X_n}$ be the flow defined by the vector field X_n. In section 2.4 we will show that $\Phi^\epsilon_{X_n} = F_\epsilon + O(\epsilon^{2n+1})$. Moreover, in a way similar to the classical averaging theory [10], the interpolation error becomes exponentially small, $O(\mathrm{e}^{-c/|\epsilon|})$, when n is chosen to be of order of ϵ^{-1}.

If $F_\epsilon : D \to D$ is a diffeomorphism, then the domain D is invariant and the equation (1.3) defines X_n on D for every $n \in \mathbb{N}$. In general, we do not assume that D is invariant, and iterates of a point $x_0 \in D$ may leave the domain. Nevertheless, it is not difficult to show that for any compact subset $D_0 \subset D$, there is a constant $r_0 > 0$ such that $x_k = F_\epsilon^k(x)$ is defined for every $x \in D_0$ and every integer k provided $|\epsilon k| \le r_0$. Therefore X_n is defined on D_0 for every $n \le r_0|\epsilon|^{-1}$.

If the map F_ϵ is a lift of a diffeomorphism of a torus or cylinder, then the interpolating vector field is also a lift of a vector field defined on the same manifold. It is possible to generalize the definition onto a general manifold but this discussion is beyond the aims of the present paper.

We note that if F_ϵ and F_ϵ^{-1} are both polynomial (e.g. the classical Hénon map and its generalisations), then the interpolating vector field is also polynomial.

In the symplectic case, the interpolating vector fields remove the need of computing an averaged Hamiltonian. This opens an opportunity of performing massive numerical explorations of a multi-dimensional phase space, reducing the computation time significantly. Possible dynamical applications of this visualizing techniques include, among others, studying of area-preserving maps in $\mathbb{C}^2$ and of Arnold diffusion for 4-dimensional symplectic maps near double resonances.

The rest of this paper is organised as follows. In Section 2 we briefly summarise the Lagrangian interpolation theory and derive some properties of the interpolating vector fields. Then we analyse the accuracy of interpolation. We discuss connections between the interpolating vector field and suspensions of the map F_ϵ. In particular, we discuss connections to averaging methods and the optimality of choosing n as a function of ϵ. We show that in the analytic case the interpolation error can become exponentially small in ϵ. Finally, in subsection 2.5 we consider the symplectic setting. Although the interpolating vector field

X_n is not symplectic, it still can be used to define an adiabatic invariant h_n which remains approximately constant for about ϵ^{-2n} iterates of the map F_ϵ.

In Section 3 we present results of our numerical experiments to illustrate the use of the interpolating vector fields for exploring the dynamics of maps in regions where they are near the identity. First, in Section 3.1 we consider the 2-dimensional symplectic case and perform experiments with the Chirikov standard map as a model. This is a preliminary example which illustrates various useful features of the interpolating vector fields. Moreover, one can compare the interpolating vector field directly with the map as the two dimensional dynamics is easy to visualize.

The main advantage of interpolating vector fields is that they provide a useful tool to investigate higher dimensional phase spaces. In particular, they provide a powerful tool for computing projections of the discrete dynamics onto subspaces of codimension-one. We use this tool to define Poincaré sections for maps, an extension of the classical construction traditionally restricted to systems with continuous time only, see details in Section 3.2. We illustrate this construction for a three-dimensional volume-preserving map and a four-dimensional symplectic map and obtain representations of different types of dynamics with the help of plots in dimensions two and three.

2 Interpolating vector fields

2.1 Lagrange interpolating polynomials

An interpolating polynomial can be explicitly written with the help of Lagrange interpolating polynomials (see e.g. [15]). Suppose that nodes are located at integer points symmetrically with respect to $\tau = 0$. Then Lagrange's fundamental interpolating polynomial is

$$\pi_n(\tau) = \prod_{k=-n}^{n} (\tau - k) \tag{2.1}$$

and Lagrange's basis polynomials are

$$\pi_{nk}(\tau) = \frac{\pi_n(\tau)}{\pi_n'(k)(\tau - k)}. \tag{2.2}$$

For every $n \in \mathbb{N}$ and $|k| \leq n$ the equation (2.2) defines the unique polynomial of degree $2n$ such that $\pi_{nk}(j) = \delta_{kj}$ for every $|j| \leq n$, where δ_{kj} is the Kronecker delta. For $1 \leq |k| \leq n$ we differentiate the equation (2.2) and, taking into account that $\pi_n(0) = 0$, we get $\pi_{nk}'(0) = -\frac{\pi_n'(0)}{k\pi_n'(k)}$. Since $\pi_n'(0) = (-1)^n(n!)^2$ and

$$\pi_n'(k) = \prod_{j=-n}^{k-1} (k - j) \prod_{j=k+1}^{n} (k - j) = (-1)^{n-k}(n + k)!(n - k)! \tag{2.3}$$

we conclude that $\pi'_{nk}(0) = p_{nk}$ where

$$p_{nk} = \frac{(-1)^{k+1}(n!)^2}{k(n+k)!(n-k)!}\,. \tag{2.4}$$

Since π_n is odd, π_{n0} is even and, consequently, $p_{n0} = \pi'_{n0}(0) = 0$. The constants p_{nk} are used in the equation (1.3) which defines the interpolating vector fields. Later we will need some properties of these constants.

Proposition 2.1. *For every n fixed, $(-1)^{k+1}p_{nk}$ is a monotone decreasing positive sequence for $1 \le k \le n$, and $p_{n,-k} = -p_{nk}$. Moreover,*

$$\sum_{k=-n}^{n} p_{nk}k^j = \begin{cases} 1, & \text{if } j = 1, \\ 0, & \text{if } j = 0 \text{ or } 2 \le j \le 2n, \end{cases} \tag{2.5}$$

$$\sum_{k=1}^{n} |p_{nk}| = \frac{H_n}{2} \qquad \text{and} \qquad \sum_{k=1}^{n} p_{nk} = H_{2n} - H_n, \tag{2.6}$$

where $H_n = \sum_{k=1}^{n} k^{-1}$ is the n-th harmonic number.

Proof. The first equality can be derived from the following observation. Let $0 \le j \le 2n$. Interpolating any polynomial of degree j with the help of a polynomial of degree $2n$, we recover the original polynomial. Applying this rule to τ^j we get that

$$\sum_{k=-n}^{n} \pi_{nk}(\tau)k^j = \tau^j.$$

Differentiating this equality with respect to τ at $\tau = 0$ we obtain (2.5). □

Let $r > 0$ and consider a continuous curve $\gamma : [-r, r] \to \mathbb{R}^m$. For any $\epsilon \neq 0$ and $n \in \mathbb{N}$ such that $n|\epsilon| < r$, the equation

$$p_n(t, \epsilon) = \sum_{k=-n}^{n} \pi_{nk}(\epsilon^{-1}t)\gamma(k\epsilon)$$

defines the unique polynomial of degree $2n$ such that $p_n(k\epsilon, \epsilon) = \gamma(k\epsilon)$ for $|k| \le n$. Let $v_n(\gamma, \epsilon) = \partial_t p_n(0, \epsilon)$. Taking into account the expression for p_n we get

$$v_n(\gamma, \epsilon) = \epsilon^{-1} \sum_{k=-n}^{n} p_{nk}\gamma(k\epsilon). \tag{2.7}$$

Note that although this definition contains a division by ϵ, the following lemma implies that v_n can be extended to $\epsilon = 0$ by continuity provided the curve is sufficiently smooth.

Lemma 2.2. *If $\gamma \in \mathcal{C}^{2n+1}\big([-r,r]\big)$ and $|\epsilon| n < r$, then*

$$|\dot\gamma(0) - v_n(\gamma,\epsilon)| \le \frac{\epsilon^{2n}(n!)^2}{(2n+1)!} \max_{|t|\le r} \left|\gamma^{(2n+1)}(t)\right|. \tag{2.8}$$

Proof. The standard theory of interpolating polynomials, see e.g. [15], states that

$$\gamma(t) = p_n(t,\epsilon) + \frac{\epsilon^{2n+1}\pi_n(\epsilon^{-1}t)}{(2n+1)!} w_n(t,\epsilon),$$

where the function w_n can be expressed as $w_n(t,\epsilon) = \gamma^{(2n+1)}(\tau_*(t,\epsilon))$ with $\tau_*(t,\epsilon) \in [-n\epsilon, n\epsilon]$, an intermediate value of the time variable. Since the zeroes of π are all simple, w is continuous at $t = k\epsilon$. Differentiating with respect to t at $t = 0$ and taking into account that $\pi_n(0) = 0$, we get

$$\dot\gamma(0) = v_n(\gamma,\epsilon) + \frac{\epsilon^{2n}\pi_n'(0)}{(2n+1)!}\gamma^{(2n+1)}(\tau_*(0,\epsilon)).$$

The estimate of the lemma immediately follows from (2.3). This inequality implies that $v_n(\gamma,\epsilon) \to \dot\gamma(0)$ when $\epsilon \to 0$. □

Lemma 2.3 (stability with respect to perturbations)**.** *If $\gamma_1, \gamma_2 \in \mathcal{C}^0([-r,r])$, $\epsilon \neq 0$ and $n|\epsilon| < r$, then*

$$|v_n(\gamma_2,\epsilon) - v_n(\gamma_1,\epsilon)| \le |\epsilon|^{-1} H_n \, \|\gamma_2 - \gamma_1\|$$

where $H_n = \sum_{k=1}^n k^{-1}$ is the n-th harmonic number.

Proof. Using (2.7) and the triangle inequality we get

$$\begin{aligned} |v_n(\gamma_2,\epsilon) - v_n(\gamma_1,\epsilon)| &\le |\epsilon|^{-1} \sum_{k=-n}^{n} |p_{nk}| \, |\gamma_2(k\epsilon) - \gamma_1(k\epsilon))| \\ &\le |\epsilon|^{-1} \, \|\gamma_2 - \gamma_1\| \sum_{k=-n}^{n} |p_{nk}|. \end{aligned}$$

Then the first equality in (2.6) implies the estimate of the lemma. □

2.2 Basic properties of interpolating vector fields

The interpolating polynomial of the equation (1.1) can be explicitly written in the form of a Lagrange interpolating polynomial, namely,

$$p_n(t,x,\epsilon) = \sum_{k=-n}^{n} \pi_{nk}(\epsilon^{-1}t) x_k, \qquad \text{where } x_k = F_\epsilon^k(x).$$

Differentiating this equality with respect to t at $t = 0$ and using that $\pi_{nk}'(0) = p_{nk}$, we recover the explicit expression (1.3) for the interpolating vector field (1.2):

$$X_n(x,\epsilon) = \epsilon^{-1} \sum_{k=-n}^{n} p_{nk} x_k = \epsilon^{-1} \sum_{k=1}^{n} p_{nk}(x_k - x_{-k}). \tag{2.9}$$

For example, for $n = 2$ we get

$$X_2(x,\epsilon) = \frac{2}{3\epsilon}\left(F_\epsilon(x) - F_\epsilon^{-1}(x)\right) - \frac{1}{12\epsilon}\left(F_\epsilon^2(x) - F_\epsilon^{-2}(x)\right).$$

The definition of the interpolating vector field involves division by ϵ, but we will see that X_n can be continuously extended to $\epsilon = 0$.

Proposition 2.4. *Let $D_0 \subset D$ be compact. Then there is $r_0 > 0$ such that the interpolating vector field is defined for all $x \in D_0$ and all $n \in \mathbb{N}$ such that $n|\epsilon| \le r_0$. For every n, the interpolating vector field X_n is as smooth as the map F_ϵ itself and $X_n(x,0) = G_0(x)$.*

Proof. Let $F_\epsilon(x) = x + \epsilon G_\epsilon(x) = x + \epsilon g_1(x,\epsilon)$. Obviously, $g_1(x,0) = G_0(x)$. Then the finite induction implies that

$$x_k = F_\epsilon^k(x) = x_0 + \epsilon \sum_{j=0}^{k-1} g_1(x_j,\epsilon) \tag{2.10}$$

for every $k \in \mathbb{N}$ such that $x_j \in D$ for all $0 \le j \le k$. Similarly, the inverse function theorem implies that $F_\epsilon^{-1}(x) = x - \epsilon g_{-1}(x,\epsilon)$, where $g_{-1}(x,0) = -G_0(x)$. Repeating the previous arguments we conclude that

$$x_{-k} = F_\epsilon^{-k} = x_0 + \epsilon \sum_{j=0}^{k-1} g_{-1}(x_{-j},\epsilon). \tag{2.11}$$

Using the finite induction, the equations (2.10) and (2.11) and compactness of D_0, we prove that there is $r_0 > 0$ such that $F_\epsilon^k(x) \in D$ for all $x \in D_0$ provided $|k\epsilon| < r_0$.

Substituting the expressions (2.10) and (2.11) into the definition (2.9) of X_n, and using (2.5) with $j = 0$, we obtain

$$X_n(x,\epsilon) = \sum_{k=-n}^{n} p_{nk} \sum_{j=0}^{|k|-1} g_{\mathrm{sign}(k)}(x_{\mathrm{sign}(k)j},\epsilon) \tag{2.12}$$

and the smoothness of X_n follows directly. Finally, we note that if $\epsilon = 0$, then $x_j = x_0 = x$ for every j. Substituting $\epsilon = 0$ into the equation (2.12) we get

$$X_n(x,0) = \sum_{k=-n}^{n} p_{nk} \sum_{j=0}^{|k|-1} g_{\mathrm{sign}(k)}(x,0) = \sum_{k=-n}^{n} p_{nk} k G_0(x).$$

Then the equation (2.5) with $j = 1$ implies that $X_n(x,0) = G_0(X)$. □

An interpolating vector field can be used to approximately restore a vector field from its time-ϵ map.

Proposition 2.5. *Let Φ^τ be a time-τ flow of a smooth autonomous vector field Y and $n \in \mathbb{N}$. Let X_n be an interpolating vector field for the map Φ^ϵ. Then*

$$Y(x) = X_n(x, \epsilon) + O(\epsilon^{2n}).$$

The estimate is uniform on every compact subset of D.

Proof. Let $x \in D$ and γ be a solution of the initial value problem for the ordinary differential equation $\dot\gamma = Y(\gamma)$, $\gamma(0) = x$. Then Proposition 2.5 follows from Lemma 2.2 as the solution is smooth. □

We note that the following arguments can also be used to prove the proposition. Expanding the solution γ of the initial value problem into Taylor series in time we get

$$\gamma(t) = x + \sum_{k=1}^{2n} \frac{t^k}{k!}\gamma^{(k)}(0) + r_{2n}(t)$$

where $\gamma^{(1)}(0) = Y(x)$ and $r_{2n}(t) = O(t^{2n+1})$. Substituting this expression into the definition of the interpolating vector field we get

$$\begin{aligned} \epsilon X_n(x,\epsilon) &= \sum_{k=-n}^{n} p_{nk}\gamma(\epsilon k) = \sum_{k=-n}^{n} p_{nk}\left(\sum_{j=1}^{2n} \frac{\epsilon^j k^j}{j!}\gamma^{(j)}(0) + r_{2n}(k\epsilon)\right) \\ &= \sum_{j=1}^{2n} \frac{\epsilon^j}{j!}\gamma^{(j)}(0) \sum_{k=-n}^{n} k^j p_{nk} + R_n(\epsilon) = \epsilon Y(x) + R_n(\epsilon), \end{aligned}$$

where $R_n(\epsilon) = \sum_{k=-n}^{n} p_{nk} r_{2n}(k\epsilon) = O(\epsilon^{2n+1})$. Here we used the equation (2.5) to simplify the sum.

Remark 2.6. *If x_0 is a fixed point of F_ϵ, then x_0 is an equilibrium of X_n.*

Remark 2.7. *For a fixed n and a small ϵ the interpolating vector field $X_n(x, \epsilon)$ only involves values of F_ϵ from a small neighbourhood of the point x.*

Remark 2.8. *If F_ϵ is a lift of a map defined on a cylinder (or a torus), then the interpolating vector field X_n is also a lift of a vector field defined on the same manifold. This argument also applies to every manifold obtained by factorising $\mathbb{R}^m$ with respect to action of a discrete group of (affine) linear transformations.*

We recall that a map F_ϵ is called *reversible*, if there is an involution R (i.e., $R \circ R = \mathrm{I}$) which conjugates the map and its inverse, i.e., $F_\epsilon^{-1} = R \circ F_\epsilon \circ R$. The involution R is called a *reversor*. In this paper we consider only the case when R is a linear map. This case is often used in applications.

Proposition 2.9. *If F_ϵ is a reversible map with a linear reversor R, then the interpolating vector field is also reversible, i.e. the application of the map R changes the direction of time:*

$$X_n(Rx) = -RX_n(x).$$

This proposition is proved by a straightforward computation using the symmetric expression for the interpolating vector field (1.3) and the fact that the reversor R maps a trajectory of F_ϵ into a trajectory of F_ϵ^{-1}.

Let F_ϵ be a map defined on an one-dimensional interval. Suppose that $x_0 \in \mathbb{R}$ is a fixed point of F_ϵ and let $\lambda_\epsilon = F_\epsilon'(x_0)$. Then x_0 is an equilibrium for the interpolating vector field, i.e. $X_n(x_0) = 0$, and

$$X_n'(x_0) = \epsilon^{-1} \sum_{k=1}^{n} p_{nk} \left(\lambda_\epsilon^k - \lambda_\epsilon^{-k}\right).$$

If ϵ is sufficiently small, the linear stability type of the fixed point is the same for the map and for the interpolating vector field. Moreover, since F_ϵ is a monotone function, it is easy to see that the time-ϵ map of the interpolating vector field is topologically conjugate to F_ϵ. On the other hand, in general, the conjugating function cannot be differentiable as the multipliers λ_ϵ and $\exp(\epsilon X_n'(x_0))$ of the fixed points can be different. The conclusions about topological equivalence do not require hyperbolicity of F_ϵ and do not generalize to higher dimensions.

2.3 Suspensions of a map and averaging

In general it is not possible to construct an autonomous vector field such that its time-ϵ map coincides with F_ϵ. On the other hand, it is possible to construct a time-periodic vector field with this property. Such vector field is called a *suspension of* F_ϵ. Suppose that Y is a suspension of F_ϵ. This vector field has the following characteristic property: if $\xi = \xi(\tau, x, \epsilon)$ is a solution of the initial value problem

$$\partial_\tau \xi = \epsilon Y(\tau, \xi, \epsilon), \qquad \xi(0, x, \epsilon) = x\,, \tag{2.13}$$

then $\xi(1, x, \epsilon) = F_\epsilon(x)$. Note that we use the fast time $\tau = \epsilon^{-1}t$ instead of the slow time t.

It is not too difficult to construct a suspension. Indeed, let $\chi : [0,1] \to [0,1]$ be a monotone smooth ($\mathcal{C}^\infty$) function, such that $\chi(0) = 0$, $\chi(1) = 1$ and $\chi^{(k)}(0) = \chi^{(k)}(1) = 0$ for all $k \in \mathbb{N}$. Then consider a curve parametrized by the function

$$\xi(\tau, x, \epsilon) = x + \epsilon\chi(\tau)G_\epsilon(x) \tag{2.14}$$

with $\tau \in [0,1]$. This curve connects the points x and $F_\epsilon(x) = x + \epsilon G_\epsilon(x)$. Consider the map $\Phi_\epsilon^\tau : x \mapsto \xi(\tau, x, \epsilon)$. This map is ϵ-close to the identity in the $\mathcal{C}^1$ topology and, hence, a local diffeomorphism by the inverse function theorem. Let $\Psi_\epsilon^\tau = (\Phi_\epsilon^\tau)^{-1}$ and consider a non-autonomous vector field

$$Y(\tau, x, \epsilon) = \chi'(\tau)G_\epsilon(\Psi_\epsilon^\tau(x)) \tag{2.15}$$

originally defined for $\tau \in [0,1]$ and extended periodically as a function of τ. It is easy to see that Y is smooth.

Obviously, the function (2.14) is a solution of the initial value problem (2.13) with the vector-field defined by (2.15). Consequently, the time-τ map of the vector field ϵY coincides with Φ_ϵ^τ for $\tau \in [0,1]$. Since $\Phi_\epsilon^1 = F_\epsilon$, the vector field Y is a suspension of the map F_ϵ.

Note that in this construction solutions of the differential equations (2.13) are given explicitly for $\tau \in [0,1]$. These solutions extend recursively to other values of τ using the identity $\xi(\tau, x, \epsilon) = \xi(\tau - 1, F_\epsilon(x), \epsilon)$. Since the function χ is flat at $\tau = 0$ and $\tau = 1$, the function ξ is smooth in time as long as the solution remains in D. It is also possible to use the flow $\Phi_\epsilon^\tau(x) = F_{\epsilon\chi(\tau)}(x)$ instead of (2.14) in the construction of the suspension.

A suspension of F_ϵ is not unique and we are interested in finding a suspension which is as close to an autonomous vector field as possible. This task can be performed with the help of averaging [2]. An averaging step consists of a substitution of the form

$$\xi = \xi_1 + S(\tau, \xi_1, \epsilon) \tag{2.16}$$

where the function S is periodic in τ. Substituting (2.16) into the differential equation (2.13) we get

$$(1 + \partial_\xi S)\partial_\tau \xi_1 + \partial_\tau S = \epsilon Y(\tau, \xi_1 + S, \epsilon) \tag{2.17}$$

where S is evaluated at (τ, ξ_1, ϵ). Let $\langle Y \rangle = \int_0^1 Y d\tau$ be the mean value of Y over its period in τ, and $\tilde{Y} = Y - \langle Y \rangle$ be its oscillatory part with zero mean. It is convenient to let

$$S(\tau, \xi, \epsilon) = \epsilon \int_0^\tau \tilde{Y}(t, \xi, \epsilon)\, dt.$$

This function is periodic in τ and $S(k, \xi, \epsilon) = 0$ for every $k \in \mathbb{Z}$. Then the map $\xi_1 \mapsto \xi$ is ϵ-close to the identity for every τ and is exactly the identity for $\tau \in \mathbb{Z}$. Therefore, the change of variables (2.16) transforms Y into another suspension of the same map F_ϵ. Multiplying the equation (2.17) by the matrix $(1 + \partial_\xi S)^{-1}$, we write the new suspension in the form

$$\partial_\tau \xi_1 = \epsilon Y_1(\tau, \xi_1, \epsilon),$$

where

$$Y_1(\tau, \xi_1, \epsilon) = (1 + \partial_\xi S)^{-1}\big(Y(\tau, \xi_1 + S, \epsilon) - \tilde{Y}(\tau, \xi_1, \epsilon)\big).$$

Taking into account that $S = O(\epsilon)$, the definition of $\tilde{Y}$ and differentiability of Y and S, we can check that the oscillatory part of Y_1 vanishes at the leading order, i.e., $\|\tilde{Y}_1\| = O(\|\epsilon\tilde{Y}\|)$. The averaging procedure can be repeated to further decrease the time-dependent part of the suspension. Note that the expression for the vector field Y_1 contains a first derivative with respect to the space variable, thus if $Y \in \mathcal{C}^k$ then we can claim that $Y_1 \in \mathcal{C}^{k-1}$ only and the maximum number of averaging steps is bounded by the smoothness class of Y. If Y is infinitely differentiable, the time-dependent part of the suspension vector field can be made smaller than any power of $|\epsilon|$ by repeating the averaging procedure multiple times: after n steps we obtain a suspension of the form

$$Y_n(\tau, x, \epsilon) = A_n(x, \epsilon) + \epsilon^n B_n(\tau, x, \epsilon). \tag{2.18}$$

Neishtadt [10] proved that if Y is analytic in a complex neighbourhood of D then after $n \sim |\epsilon|^{-1}$ averaging steps the time-dependent part of the suspension vector field becomes

exponentially small compared to $|\epsilon|$. I.e., if F_ϵ is a family of maps analytic in a complex neighbourhood of D, then there is a suspension vector field defined on D such that

$$Y(\tau, x, \epsilon) = A(x, \epsilon) + B(\tau, x, \epsilon), \tag{2.19}$$

with $B = O(\exp(-c/|\epsilon|))$ for some $c > 0$.

2.4 Suspensions of a map and interpolating vector fields

Although the averaging is an effective tool for studying near identity maps, it is not usually possible to find an explicit expression for the vector fields Y_n.

Theorem 2.10. *Let $F_\epsilon : D \to \mathbb{R}^m$ be a smooth family of near identity maps defined on a domain $D \subset \mathbb{R}^m$ with $m \geq 1$ and let $n \in \mathbb{N}$. If a suspension of F_ϵ can be written in the form*

$$Y(t, x, \epsilon) = A_n(x, \epsilon) + \epsilon^{2n} B_n(t, x, \epsilon) \tag{2.20}$$

where the $\mathcal{C}^{2n}$ norms of A_n and B_n are bounded uniformly with respect ϵ, then for every compact $D_0 \subset D$ there is a constant C_n such that

$$\sup_{x \in D} |A_n(x, \epsilon) - X_n(x, \epsilon)| \leq C_n \epsilon^{2n}$$

where X_n is the interpolating vector field for the map F_ϵ.

Proof. Since D_0 is compact, there is $\epsilon_0 > 0$ such that every solution of

$$\partial_\tau \xi(\tau, x, \epsilon) = \epsilon Y(\tau, \xi(\tau, x, \epsilon), \epsilon), \qquad \xi(0, x, \epsilon) = x \tag{2.21}$$

with initial condition $x \in D_0$ remains inside D for $|\tau| \leq n$ and $|\epsilon| \leq \epsilon_0$. Since Y is a suspension of F_ϵ, we have $F_\epsilon^k(x) = \xi(k, x, \epsilon)$ for $|k| \leq n$. Repeatedly differentiating the equation (2.21) with respect to τ and taking into account the form of Y, we see that there is a constant C such that

$$\left|\partial_\tau^k \xi(\tau, x, \epsilon)\right| \leq C|\epsilon|^k$$

for $k \leq 2n + 1$. Then the theorem follows from the Lemma 2.2 with $\gamma(t) = \xi(\epsilon^{-1}t, x, \epsilon)$. □

This theorem has several important corollaries. The first one states that the time-ϵ shift along trajectories of the interpolating vector field approximates F_ϵ.

Corollary 2.11. *If $F_\epsilon \in \mathcal{C}^{2n+1}$ and D_0 is a compact subset of D then on this subset the interpolating vector field is uniformly bounded for $|\epsilon| < \epsilon_0$ and*

$$F_\epsilon(x) = \Phi^\epsilon_{X_n}(x) + O(\epsilon^{2n+1})$$

where $\Phi^\epsilon_{X_n}$ is the time-ϵ map associated with the vector field X_n.

If F_ϵ is analytic in a complex neighbourhood of D_0, then we can choose $n \sim |\epsilon|^{-1}$ in order to obtain a vector field which interpolates F_ϵ with an error exponentially small in ϵ. To prove this, let Y be the suspension of F_ϵ given by (2.19). So its non-autonomous part B is exponentially small in ϵ. Suppose that a solution of the autonomous equation $\partial_t \eta(t, x, \epsilon) = A(\eta, \epsilon)$ with $\eta(0, x, \epsilon) = x \in D_0$ is analytic in time for $|t| < 3r$ because it remains inside the domain of the vector field A for these values of t. Then the Cauchy estimate implies that $|\partial_t^{k+1}\eta| \leq k! r^{-k} \|A\|$ for $|t| \leq r$. Let $\tilde{X}_n(x, \epsilon)$ be the interpolating vector field for the time-ϵ map of the flow of A. Applying Lemma 2.2 to the curve $\gamma(t) = \eta(t, x, \epsilon)$, we obtain that for $n|\epsilon| < r$

$$\left| A(x, \epsilon) - \tilde{X}_n(x, \epsilon) \right| \leq \frac{\epsilon^{2n} (n!)^2}{2n+1} r^{-2n} \|A\|.$$

Then Stirling's formula implies

$$\left| A(x, \epsilon) - \tilde{X}_n(x, \epsilon) \right| \leq \left(\frac{\epsilon n}{re} \right)^{2n} \frac{4\pi n}{2n+1} \|A\|.$$

Since B is small, the time-t map of A is close to the time-t map of Y. In particular, Lemma 2.3 implies that

$$\left| X_n(x, \epsilon) - \tilde{X}_n(x, \epsilon) \right| \leq H_n |\epsilon|^{-1} C_A \|B\|.$$

where $C_A > 0$ is a suitable constant so that $C_A \|B\|$ bounds the distance between the solutions of the initial value problems related to the vector fields A and Y for $|t| \leq r$. Using the triangle inequality we get

$$|A(x, \epsilon) - X_n(x, \epsilon)| \leq \left(\frac{\epsilon n}{re} \right)^{2n} \frac{4\pi n}{2n+1} \|A\| + H_n |\epsilon|^{-1} C_A \|B\|.$$

Since $B = \mathcal{O}(e^{-c/|\epsilon|})$ for a suitable $c > 0$ it follows that, taking $n = [r/|\epsilon|]$, one obtains

$$|A(x, \epsilon) - X_n(x, \epsilon)| \leq 2\pi \|A\| e^{-r/|\epsilon|} + |\epsilon|^{-1} \log |\epsilon|^{-1} C e^{-c/|\epsilon|}.$$

Thus for this $n = n(\epsilon)$ the vector field X_n interpolates the map with an error exponentially small in ϵ.

2.5 Adiabatic invariants of a symplectic map

Let $m = 2d$ and ω be a symplectic form on $\mathbb{R}^{2d}$. We will mainly consider the standard symplectic form

$$\omega = \sum_{i=1}^{d} dx_i \wedge dx_{i+d}.$$

A map is called *symplectic* if it preserves ω. Even when F_ϵ is symplectic, the corresponding interpolating vector field X_n does not necessary define a symplectic flow and, consequently, is

not necessarily Hamiltonian. Therefore there is no reason to expect that X_n has an integral. Nevertheless, X_n is very close to a symplectic one and can be used to define an adiabatic invariant – a function which is approximately preserved on time scales much longer than $|\epsilon|^{-1}$.

In order to construct the adiabatic invariant, we consider a differential one-form $\nu_n = \omega(X_n, \cdot)$. In the case of the standard symplectic form

$$\nu_n = \sum_{i=1}^{d} \left(X_n^i dx_{i+d} - X_n^{i+d} dx_i \right), \tag{2.22}$$

where X_n^i denotes a component of the vector X_n. Then we fix a base point $x_b \in D$ and, for every $x \in D$, consider an integral

$$h_n(x, \epsilon) = \int_{\gamma(x_b, x)} \nu_n \tag{2.23}$$

where $\gamma(x_b, x)$ is a curve which connects the base point x_b and x. If the form ν_n is closed and the domain D is simply connected, this integral does not depend on the choice of the path (yet it depends on the choice of x_b) and uniquely defines the function $h_n : D \to \mathbb{R}$ such that $dh_n = \nu_n$.

In general, the form ν_n is not necessarily closed and the integral may depend on the choice of the path. In order to obtain a well-defined function we choose a rule for selecting $\gamma(x_b, x)$. For example, if the domain D is star-shaped (e.g. convex), then γ can be a straight segment connecting its end points. Another convenient choice is a path which consists of straight segments parallel to coordinate axes.

In contrast with the interpolating vector fields, a suspension vector field (2.20) for symplectic map can be chosen (locally) Hamiltonian [10, 7].

Proposition 2.12. *Let F_ϵ be a smooth family of near identity symplectic maps defined on a domain $D \subset \mathbb{R}^{2d}$ with $d \geq 1$ and let $n \in \mathbb{N}$. Let $C > 0$ be a constant and $\gamma(x_b, x)$ be piecewise smooth paths such that $|\gamma(x_b, x)| \leq C|x - x_b|$ for every $x \in D$. If a suspension of F_ϵ can be written in the form of a Hamiltonian vector field with a Hamiltonian function*

$$h(t, x, \epsilon) = h_n^a(x, \epsilon) + \epsilon^{2n} h_n^b(t, x, \epsilon)$$

where the $\mathcal{C}^{2n+1}$ norms of h_n^a and h_n^b are bounded uniformly with respect ϵ and $h_n^a(x_b, \epsilon) = 0$, then for every compact $D_0 \subset D$ there is a constant C_n such that

$$\sup_{x \in D_0} |h_n(x, \epsilon) - h_n^a(x, \epsilon)| \leq C_n \epsilon^{2n}$$

where h_n is defined by (2.23).

Proof. Let the path $\gamma(x_b, x)$ be parametrized by a function $\gamma(t, x_b, x)$ with $t \in [0, 1]$, $\gamma(0, x_b, x) = x_b$ and $\gamma(1, x_b, x) = x$. Then (2.23) takes the form

$$h_n(x, \epsilon) = \int_0^1 \omega\big(X_n(\gamma(t, x_b, x), \epsilon), \partial_t \gamma(t, x_b, x)\big) dt.$$

Let A_n be the Hamiltonian vector field defined by the Hamiltonian function h_n^a. Then

$$h_n^a(x,\epsilon) = \int_0^1 \omega\big(A_n(\gamma(t,x_b,x),\epsilon), \partial_t\gamma(t,x_b,x)\big)dt.$$

Using the bi-linearity of the symplectic form ω, we obtain

$$h_n(x,\epsilon) - h_n^a(x,\epsilon) = \int_0^1 \omega\big(X_n(\gamma(t,x_b,x),\epsilon) - A_n(\gamma(t,x_b,x),\epsilon), \partial_t\gamma(t,x_b,x)\big)dt.$$

Since $|\omega(v_1,v_2)| \le C_\omega |v_1|\,|v_2|$ for any two vectors v_1, v_2 (e.g. $C_\omega = 1$ for the standard symplectic form), we get

$$|h_n(x,\epsilon) - h_n^a(x,\epsilon)| \le C_\omega \sup_{\tilde{x}\in\gamma(x_b,x)} \big|X_n(\tilde{x},\epsilon) - A_n(\tilde{x},\epsilon)\big|\,|\gamma(x_b,x)|.$$

The proposition follows directly from Theorem 2.10. □

Corollary 2.13. *For any compact $D_0 \subset D$ and $\forall x \in D_0$, one has*

$$h_n(F_\epsilon(x),\epsilon) - h_n(x,\epsilon) = O(\epsilon^{2n}).$$

Proof. Since $F_\epsilon - \Phi^\epsilon_{A_n} = O(\epsilon^{2n+1})$, we get

$$h_n(F_\epsilon(x),\epsilon) = h_n^a(F_\epsilon(x),\epsilon) + O(\epsilon^{2n}) = h_n^a(\Phi^\epsilon_{A_n}(x),\epsilon) + O(\epsilon^{2n}).$$

The flow of A_n preserves h_n^a, in particular $h_n^a(\Phi^\epsilon_{A_n}(x),\epsilon) = h_n^a(x,\epsilon)$, and the desired estimate follows. □

This corollary implies that h_n is an adiabatic invariant of the map F_ϵ, as it is approximately preserved for ϵ^{-2n} iterations of the map, provided the corresponding segment of the trajectory remains inside D. We expect that in the case of an analytic map, the adiabatic invariant $h_{n(\epsilon)}$ is preserved over exponentially long times where $n(\epsilon) \sim |\epsilon|^{-1}$.

We note that the function h_n can be as smooth as the interpolating vector field (provided the paths $\gamma(x_b,x)$ are chosen appropriately). If the domain D is not simply-connected, the function h_n can become multivalued if it does not return to the original value when x makes a round along a closed non-contractible loop.

3 Numerical study of dynamics using interpolating vector fields

3.1 Two-dimensional area-preserving maps: the Chirikov standard map

Our first example is the Chirikov standard map [4] written in the form

$$M_\epsilon : (x,y) \mapsto (\bar{x},\bar{y}) = (x + \epsilon\bar{y}, y - \epsilon\sin(x)), \tag{3.1}$$

where ϵ is a real parameter. We consider this map on the cylinder $\mathbb{S}^1 \times \mathbb{R}$. On every bounded subset of the cylinder, the map (3.1) is close to identity provided $|\epsilon|$ is small enough.

In our first numerical experiment we take $\epsilon = 0.1$, $n = 5$ and study the interpolating vector field X_n defined by equation (1.2). We choose some initial conditions on the cylinder and compare their iterates under the original map M_ϵ with the iterates under the time-ϵ map $\Phi^\epsilon_{X_n}$ corresponding to the interpolating vector field X_n. Fig. 2 shows the first 10^3 iterates for 200 initial conditions. Both pictures use the same set of initial conditions. The interpolating vector field is integrated up to $\tau = 10^3$ with the help of a Runge-Kutta-Felberg 7-8 integrator with variable step size (RK78). There is no visually perceptible difference between the two images.

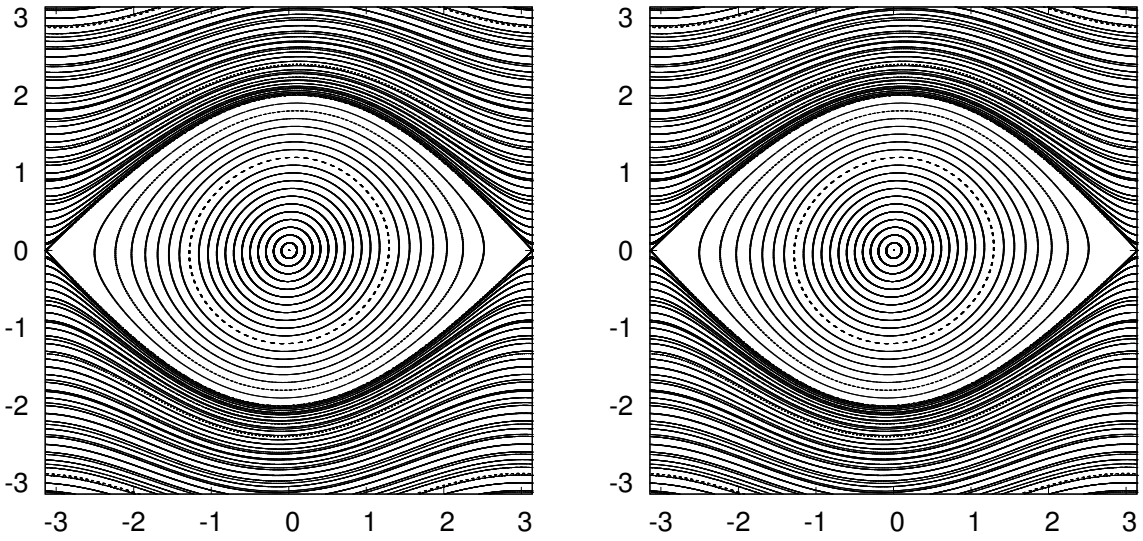

Figure 2: Iterates of the standard map M_ϵ (left) and of the time-ϵ map $\Phi^\epsilon_{X_n}$ associated to the interpolating vector field (with $n = 5$) (right). In both cases $\epsilon = 0.1$. No visual differences are detected in the plots.

In order to quantitatively describe the difference between the map and its interpolating flow, we consider interpolating vector fields X_n for $n = 5, 10, 15$ and 20. Fig. 3 shows level plots of $|\Phi^\epsilon_{X_n}(x_0) - M_\epsilon(x_0)|$ computed for 5×10^5 initial conditions selected on a uniform mesh in $[-\pi, \pi] \times [-2\pi, 2\pi]$. We clearly see that the error vanishes at the fixed points of the map and that the error decreases as n increases. Of course, the interpolation error will eventually grow with n due to Runge oscillations in interpolation.

Remark 3.1. *For the standard map (3.1), the interpolating flow X_n, for any n, defines a one degree of freedom Hamiltonian system (with a non-standard symplectic form). This follows from the fact that the map is reversible, hence so is the interpolating vector field, see Proposition 2.11. The reversibility of X_n forces the phase space to be foliated by periodic orbits, see Fig. 2 right and also the right plots of Fig. 4 as illustrations. A reversible 2-*

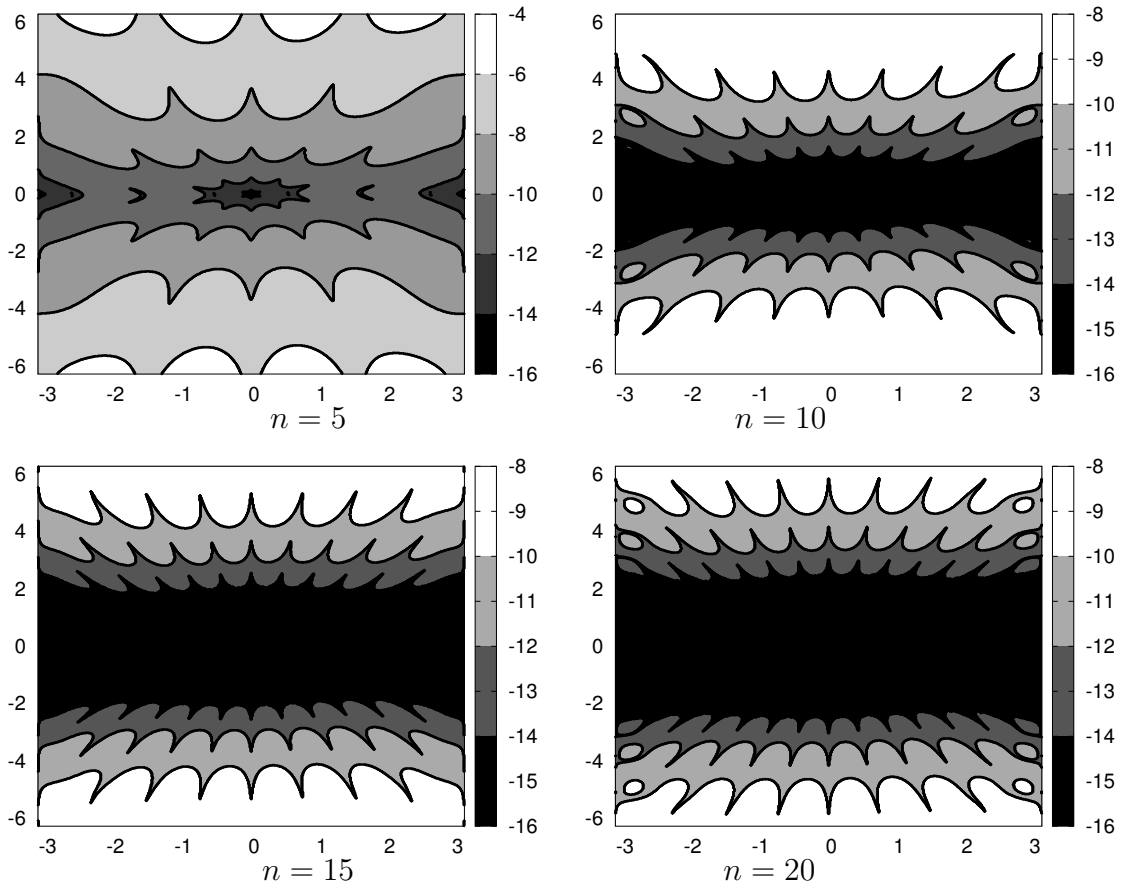

Figure 3: $\epsilon = 0.1$. Level plots of $\log_{10} |\Phi^{\epsilon}_{X_n}(x_0) - M_{\epsilon}(x_0)|$ for $x_0 \in [-\pi, \pi] \times [-2\pi, 2\pi]$, and four different values of n.

dimensional system having a foliation of periodic orbits is Hamiltonian (possibly with a non-standard symplectic form).

To visually inspect the differences between the orbits for the map and the interpolating flow, we increase the parameter up to $\epsilon = 0.5$ and show the results in Fig. 4. The left plots represent the iterates of the standard map M_{ϵ}, while the right ones correspond to the time-ϵ map $\Phi^{\epsilon}_{X_n}$ for $n = 10$. We recall that X_n defines an integrable vector field, see Remark 3.1. The bottom raw of Fig. 4 shows magnifications of a part of the pictures from the top row: we can clearly see the differences between the phase portraits when magnifying a strip located near a chain of resonant islands of the map.

To study the adiabatic invariants defined by the equation (2.23), we fix a base point $x_b \in \mathbb{R}^{2d}$ ($d = 1$ in this section but we will also use $d = 2$ later) and consider paths represented by the function $\gamma(s, x_b, x) = x_b + sv$ where $v = x - x_b$ and $0 \leq s \leq 1$. Then the

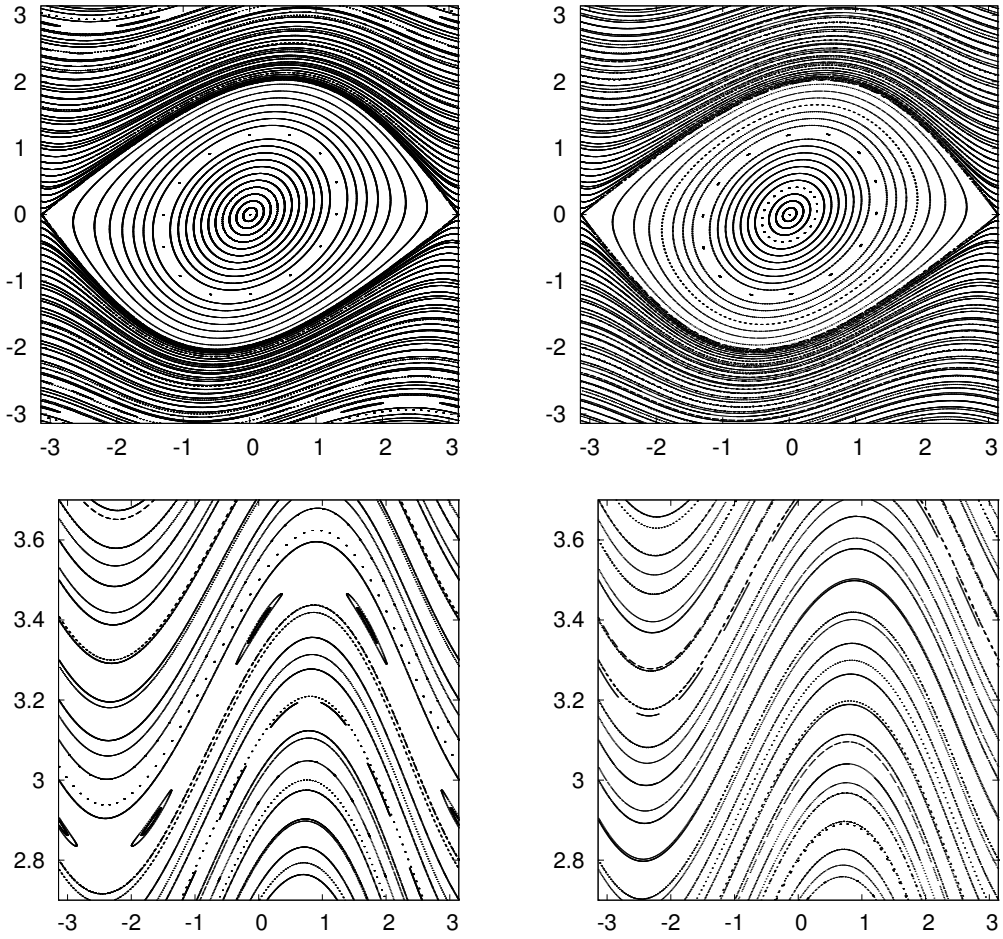

Figure 4: $\epsilon = 0.5$. Left: Iterates of the standard map M_ϵ. Right: Iterates of the time-ϵ map $\Phi^\epsilon_{X_n}$ (with $n = 10$) associated to the interpolating vector field.

integral (2.23) takes the form

$$h_n(x,\epsilon) = \int_0^1 \sum_{i=1}^{d} \left(X_n^i(\gamma(s,x_0,x),\epsilon)v_{i+d} - X_n^{i+d}(\gamma(s,x_0,x),\epsilon)v_i \right) ds \tag{3.2}$$

where v_i are components of the vector v. In numerical experiments, we evaluate this integral using a trapezoidal rule combined with the Romberg extrapolation scheme. We accept a numerical estimate of the integral value if the difference between two consecutive approximations of the Romberg scheme is less than 10^{-8}. We use this rule to evaluate the adiabatic invariants in all examples presented in the paper unless otherwise stated. In principle, this method can be used to achieve higher precision, however for the visualization purposes higher precision is not needed.

To investigate the preservation of the adiabatic invariants as a function of n and ϵ under iterates of M_ϵ, we select 10^4 initial conditions which form a uniform mesh in $[-\pi,\pi]^2$ and

for every point compute $\Delta h_n(x_0) = |h_n(M_\epsilon(x_0), \epsilon) - h_n(x_0, \epsilon)|$ and use the corresponding maximum value to estimate the supremum norm $\|\Delta h_n\|$. The point $x_b = (0, 0)$ is used as a base point in computations of h_n.

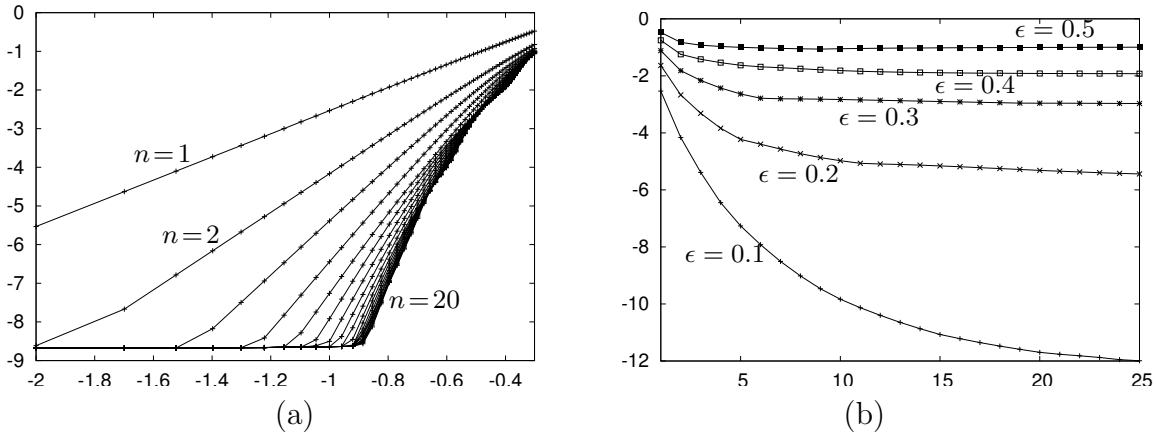

(a) (b)

Figure 5: Plots of $\log_{10} \|\Delta h_n\|$: (a) as a function of $\log_{10} \epsilon$ for $1 \le n \le 20$, and (b) as a function of n for $\epsilon = 0.1(0.1)0.5$.

Fig. 5(a) shows plots of $\|\Delta h_n\|$ as a function of $\log_{10} \epsilon$ for every $1 \le n \le 20$. Each line of the plot corresponds to a fixed value of n and is obtained by joining 50 points with different values of $\epsilon \in [0, 1/2]$. In this plot $n = 1$ corresponds to the largest values of $\|\Delta h_n\|$. This plot confirms that the upper bound of Corollary 2.13 is not too far from being optimal as the lines on the plot are approximately linear with the slope about $2n+1$ (till they reach the levelled floor located just below 10^{-8}, which is determined by our choice of the accuracy in evaluation of h_n). For $\epsilon \approx 0.15$ the values of $\|\Delta h_n\|$ are monotone decreasing for $1 \le n \le 20$. On the other hand, we see that $\|\Delta h_n\|$ is not necessarily monotone in n for larger values of ϵ as the lines have intersection. Moreover, the plot indicates that for a fixed ϵ the value of $\|\Delta h_n\|$ cannot be moved below a certain threshold by increasing the value of n (see Fig 5(b)). Therefore for a fixed ϵ we can find an optimal value of n which corresponds to a point after which the adiabatic invariant is not improved when n is increased. The existence of this threshold can be attributed to the non-integrability of the map M_ϵ. A similar phenomena are observed in the study of optimal truncation of asymptotic series.

Finally, we note that the methods of this section can be used to study some maps which are not a priori near identity but have an iterate which is near identity on some subset of the phase space. In particular, this situation can arise in a study of a near integrable system near a multiple resonance. For example, if ϵ is not small, the map M_ϵ is no longer close to identity. Nevertheless, in a neighbourhood of a q-periodic point, the map M_ϵ^q becomes close to identity. Let us illustrate how the interpolating vector field can be adapted to study the dynamics near a q-resonant chain of islands. Let $\epsilon = 0.5$. We established (see Fig. 4) that the interpolating vector field provides an accurate approximation of the dynamics of M_ϵ for $y \in [-3, 3]$. Now we consider larger values of y and investigate what happens with the

approximation. We take initial points with $x = \pi$ and iterate them. Comparing Fig 6 (a) and (b) which represent the dynamics of M_ϵ and the interpolating vector field X_n for $n = 5$, respectively, we see that the interpolating vector field does not correctly capture the dynamics around the 2-periodic chain of islands. On the other hand, in this part of the phase space the dynamics of M_ϵ^2 is sufficiently close to identity so that the interpolating vector field $X_{2,n}$, computed from iterates of M_ϵ^2, provides a good approximation of the dynamics as can be seen in Fig 6(c). Note, that only one of the two islands can be seen due to the choice of initial conditions.

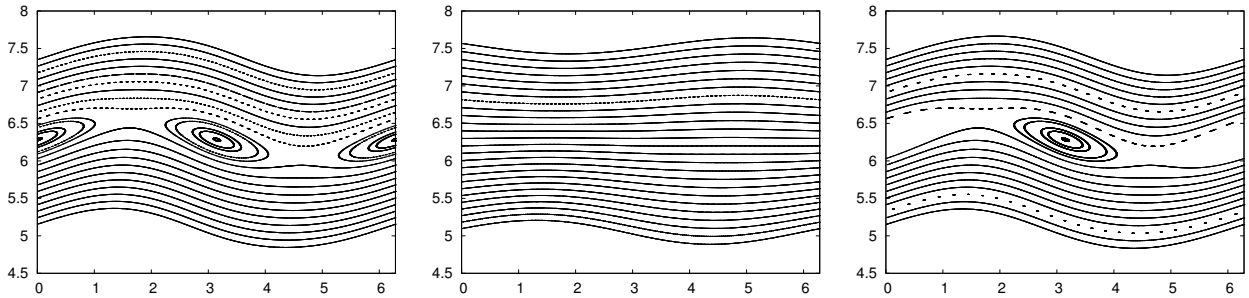

Figure 6: $\epsilon = 0.5$. Initial points taken on $x = \pi$, $n = 5$. (a) Iterates of the standard map M_ϵ, (b) Iterates of $\Phi^\epsilon_{X_n}$, and (c) Iterates of the map $\Phi^\epsilon_{X_{2,n}}$ associated with the interpolating vector field for M_ϵ^2.

Fig. 7 shows similar results for $q = 3$. Here we take initial points with $x = 0$, hence only one of the 3-periodic islands appears in the picture. The interpolating vector field X_n^3 computed for M_ϵ^3 accurately describes the dynamics in a narrow zone around the resonant 3-periodic island. Note that the 5-periodic island observed in Fig. 7(a) is not present in Fig. 7(b).

3.2 Exploring higher dimensional phase spaces: Poincaré sections for maps

If the dimension of the phase space $m \geq 3$, the visualization of the dynamics becomes more difficult. In the case of a system with continuous time, a Poincaré section provides a convenient tool to reduce the dimension: a trajectory is represented by its intersections with a codimension one surface. In the case of discrete time, the reduction of the dimension cannot be performed in a similar way. A typical solution to this problem is either to plot a projection of the trajectory on a subset of lower dimension, or to use the method of slices [12], i.e. to plot only a part of the trajectory which consists of points from a narrow strip near a codimension one surface (called a slice). In the last case, the points are also projected on the surface to reduce the dimension.

The interpolating vector fields provide a new tool for visualization of dynamics which is especially effective in dimensions three and four. Suppose that $g : \mathbb{R}^m \to \mathbb{R}$ is a smooth

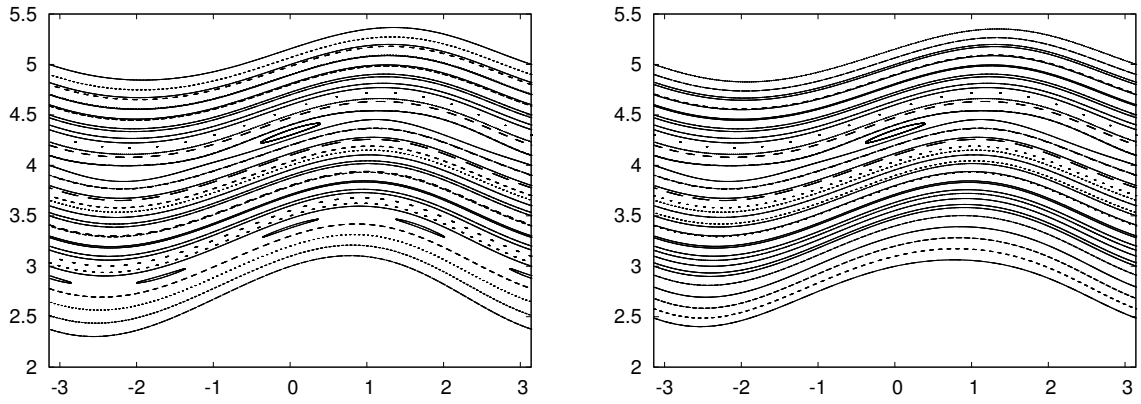

Figure 7: $\epsilon = 0.5$. Initial points taken on $x = 0$, $n = 5$. (a) Iterates of the standard map, and (b) iterates of $\Phi^{\epsilon}_{X_{3,n}}$ associated to the interpolating vector field for M^3_ϵ.

function such that its zero set $\Sigma = \{x \in \mathbb{R}^m : g(x) = 0\}$ is a smooth hyper-surface of codimension one. Taking an initial condition $x_0 \in D$ we compute the points $x_{k+1} = F_\epsilon(x_k)$ recursively. The surface Σ locally divides the space. So we can look for consecutive points of the trajectory which are separated by Σ, i.e.,

$$g(x_k)g(x_{k+1}) \leq 0. \tag{3.3}$$

Suppose that the limit vector field G_0 is transversal to Σ (at least in a neighbourhood of the intersection of Σ with the straight segment with endpoints at x_k and x_{k+1}). Then, for ϵ small enough, there is a unique $t_k \in [0, \epsilon]$ such that $g(\Phi^{t_k}_{X_n}(x_k)) = 0$, and we plot the point

$$y_k = \Phi^{t_k}_{X_n}(x_k) \tag{3.4}$$

instead of x_k. Obviously, $y_k \in \Sigma$ and the trajectory is represented on a manifold of lower dimension. The point y_k is $O(\epsilon)$ close to x_k and the error does not accumulate when k grows as the construction of y_k does not affect the computation of the trajectory $(x_k)_{k\geq 0}$.

3.3 Three-dimensional volume-preserving maps

Our next example is the 3-dimensional volume preserving map

$$G_\varepsilon : \begin{pmatrix} x \\ y \\ z \end{pmatrix} \mapsto \begin{pmatrix} \bar{x} \\ \bar{y} \\ \bar{z} \end{pmatrix} = \begin{pmatrix} x + y \\ y + \bar{z} \\ z - \varepsilon - 2.4y + x^2 + xy/2 + y^2/2 \end{pmatrix} \tag{3.5}$$

extensively studied in [5]. This map is not close to the identity. Nevertheless we can identify a part of the phase space where our interpolating vector fields can be used to study its dynamics. In [5], Dullin and Meiss showed that for $\varepsilon \in [0.01, 0.31]$ the map G_ϵ has an elliptic

invariant curve with rotation number that increases with ε and ranges in $(0.2821, 0.2853)$. The invariant curve is located at the centre of a "bubble of stability" which has a topological structure that resembles discrete spherical Hill's vortex with the rotational symmetry axis located near the x-axis. This suggests to use $\Sigma = \{z = 0\}$ as a transversal section. Here, we illustrate how to use the interpolating vector field to visualize the dynamics in Σ and compare the results with the method of slices. In all examples below, we use interpolating vector fields with $n = 5$.

We note that the rotation number of the elliptic invariant curve is relatively close to $2/7 = 0.2857\ldots$ for the specified values of ε. This implies that G_ε^7 is close to the identity in a neighbourhood of the curve. Note that the parameter ε does not measure the distance from G_ε^7 to the identity.

First we take $\varepsilon = 10^{-2}$. We consider 17 initial points $(0, 10^{-2}j, 0)$, $0 \le j \le 16$ (for initial conditions of this form with $y \ge 0.17$ the corresponding orbits are not bounded). Fig. 8 (a) shows a representation of the dynamics with the help of the method of slices: each initial condition is iterated 10^7 times and a projection on Σ is plotted for every iterate which is within the slice $|z| \le 10^{-4}$. Note that the large number of iterates is needed as only a small fraction of points lands inside the thin slice. A thicker slice would require less iterates but some details of the picture would not be visible as the projection along the z-axis does not take into account the dynamics of the map. Compare this picture with Fig. 8 (b) which is obtained with the help of the interpolating vector field: every initial condition is iterated 5×10^3 times under $G_{0.01}^7$ and, each time the trajectory crosses Σ, we project the corresponding iterate onto Σ along the interpolating vector field as explained in Section 3.2. Apparently, we obtain a comparable resolution of dynamics using each of the methodologies. Note that the number of iterates of $G_{0.01}$ needed for the method based on the interpolation vector field is smaller by more than two orders of magnitude as every passage near Σ is used to generate a point on the plot.

Next we consider $\varepsilon = 0.128$. We note that at $\varepsilon = \varepsilon_{1/4}$, where $0.12 \le \varepsilon_{1/4} \le 0.122$, the elliptic invariant curve crosses the $(4, -4, 1)$ resonance, see [5] for further details. Accordingly, for the value $\varepsilon = 0.128$ one expects to observe a related 4-periodic structure. We choose $(0, 0.41+0.005\,j, 0)$, $0 \le j \le 30$, as initial conditions, and again we compare the results of the method of slices with the method based on the interpolating vector fields. For the method of slices we perform 10^8 iterates of each condition and we display those with $|z| \le 10^{-4}$. For the computation of the Poincaré iterates using the interpolating vector field, we perform 10^3 iterates of $G_{0.128}^{28}$ and display the projections onto Σ at every crossing. The results are shown in Fig. 9 first row. We can identify clearly the 4-periodic structure in both pictures. The fact that the secondary periodic structures around this main 4-periodic one are not well-described is due to the fact that the map $G_{0.128}^{28}$ is not close enough to the identity in that region.

As a final illustration, we consider $\varepsilon = 0.252$ for which a 3-periodic structure appears. This is related to the crossing of the $(10, 3, 3)$ resonance, see [5]. We consider initial conditions $(0, 0.41 + 0.005\,j, 0)$, $0 \le j \le 40$ (some of them give rise to unbounded orbits). As before, we compare both methodologies. For the construction of the interpolating vector field we

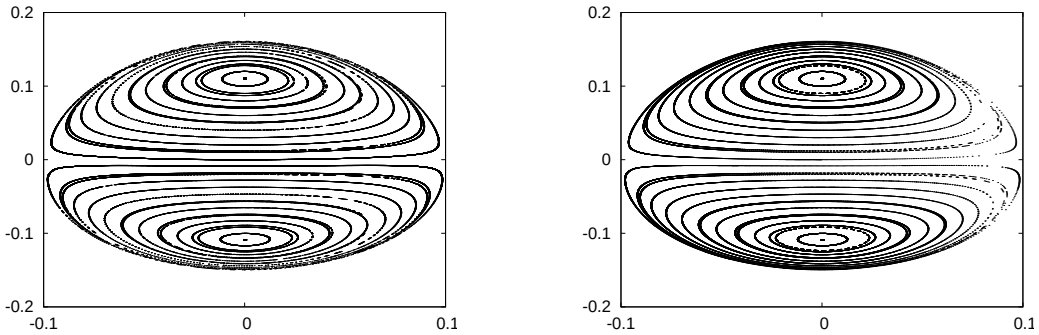

Figure 8: Both plots correspond to iterates of the same 17 initial conditions. (a) Method of slices: $N = 10^7$ iterates of $G_{0.01}$ are computed and we show orthogonal projections of iterates with $|z| \leq 10^{-4}$. (b) Method of interpolating vector fields: $N = 5 \times 10^3$ iterates of $G_{0.01}^7$ are computed, we show the projections onto Σ every time when Σ separates two consecutive iterates.

consider the map $G_{0.252}^{21}$ which is considered globally as a near identity map. The obtained visualizations of the dynamics are shown in Fig. 9 second row.

Those visualizations show that most of the details in the whole stability domain of G_ε can be detected, with a reasonable resolution, from a relativelly small number of iterates of some initial conditions using the interpolating vector field to project onto Σ.

3.4 Four-dimensional symplectic maps: the Froechlé-like map

We apply the construction of the previous section to a 4-dimensional symplectic map and show that the method reveals interesting details of the dynamics. We consider the Froechlé-like map

$$T_\epsilon : \begin{pmatrix} \psi_1 \\ \psi_2 \\ J_1 \\ J_2 \end{pmatrix} \mapsto \begin{pmatrix} \bar{\psi}_1 \\ \bar{\psi}_2 \\ \bar{J}_1 \\ \bar{J}_2 \end{pmatrix} = \begin{pmatrix} \psi_1 + \epsilon(a_1 \bar{J}_1 + a_2 \bar{J}_2) \\ \psi_2 + \epsilon(a_2 \bar{J}_1 + a_3 \bar{J}_2) \\ J_1 - \epsilon \sin(\psi_1) \\ J_2 - \epsilon\eta \sin(\psi_2) \end{pmatrix}, \tag{3.6}$$

where $a_1, a_2, a_3, \eta, \epsilon$ are real parameters. The map T_ϵ is a symplectic diffeomorphism of the cylinder $M = \mathbb{T}^2 \times \mathbb{R}^2$. It was introduced in [8] to model the dynamics near a double resonance in a near-integrable Hamiltonian system with three degrees of freedom. In our numerical experiments we use

$$a_1 = 1, \qquad a_2 = 1/2, \qquad a_3 = 5/4, \qquad \eta = 1/2. \tag{3.7}$$

The quadratic form $a_1 J_1^2 + 2a_2 J_1 J_2 + a_3 J_2^2$ is positive definite, since $a_3 - a_2^2 > 0$. The map (3.6) has four fixed points. If ϵ is positive and not too large, the origin $p_1 = (0, 0, 0, 0)$ is elliptic-elliptic, $p_2 = (0, \pi, 0, 0)$ and $p_3 = (\pi, 0, 0, 0)$ are hyperbolic-elliptic and $p_4 = (\pi, \pi, 0, 0)$ is hyperbolic-hyperbolic.

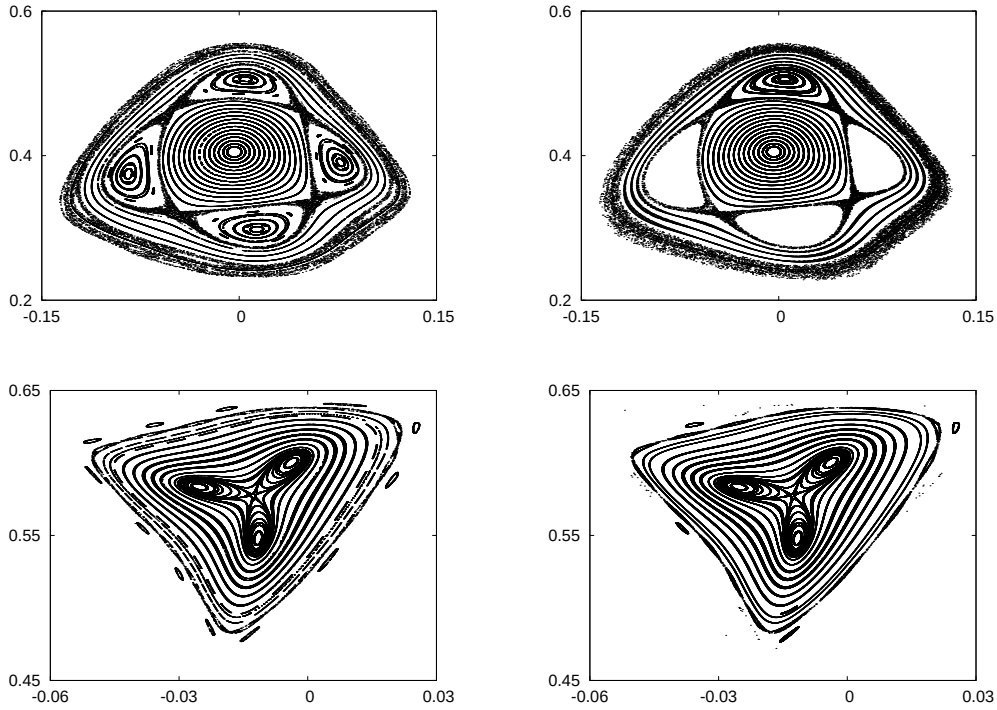

Figure 9: The plots in the left column are obtained by the method of slices, the plots in the right column are obtained with the help of interpolating vector fields. Left: We perform $N = 10^8$ iterates of each initial condition under $G_{0.128}$ (first row) and under $G_{0.252}$ (second row). We show orthogonal projections of those iterates which are within the slice $|z| \leq 10^{-4}$. Right: We perform $N = 10^4$ iterates of each initial condition under $G_{0.128}^{28}$ (first row) and under $G_{0.252}^{21}$ (second row). We display the projections along the interpolating vector field onto Σ every time that two consecutive iterates cross the section.

A Poincaré section for T_ϵ

Since the map (3.6) is symplectic, its limit flow is Hamiltonian. It is easy to find the corresponding Hamiltonian function explicitly:

$$h_0(\psi_1, \psi_2, J_1, J_2) = a_1 \frac{J_1^2}{2} + a_2 J_1 J_2 + a_3 \frac{J_2^2}{2} - \cos(\psi_1) - \eta \cos(\psi_2). \tag{3.8}$$

This Hamiltonian defines a non-integrable Hamiltonian system with two degrees of freedom. The Hamiltonian h_0 has four critical points which coincide with the fixed points of T_ϵ. Levels of constant energy, $M_E^0 = \{x : h_0(x) = E\}$, are smooth hyper-surfaces for every regular value of h_0. It is natural to study the dynamics of the limit system restricted on each energy level separately as the Hamiltonian function h_0 remains constant along trajectories of the limit flow. Let Σ be the 3-dimensional hyper-surface defined by the equality $\psi_1 = \psi_2$. Note that we do not call Σ a "hyper-plane" because we treat ψ_1 and ψ_2 as angular variables. The limit vector field is transversal to Σ except for points which satisfy the equation $(a_1 - a_2)J_1 = (a_3 - a_2)J_2$ where the vector field is tangent to Σ.

The intersection $\Sigma_E^0 = \Sigma \cap M_E^0$ defines a Poincaré section for the limit flow. Outside a neighbourhood of the tangencies, the first return map of the limit flow defines an area-preserving map on Σ_E^0. The dynamics of the limit Hamiltonian system are described by a collection of the Poincaré sections for different values of E. Since the quadratic form $a_1 \frac{J_1^2}{2} + a_2 J_1 J_2 + a_3 \frac{J_2^2}{2}$ is positive definite, M_E^0 is diffeomorphic to a three dimensional torus $\mathbb{T}^3$ for every $E > h_0(p_4) = 1 + \eta$. Then Σ_E^0 is diffeomorphic to a two dimensional torus $\mathbb{T}^2$. It is convenient to use $\psi = \psi_1 = \psi_2$ and $\phi = \arg(J_1 + iJ_2)$ as coordinates on Σ_E^0.

In contrast to the limit flow, the map T_ϵ does not have a first integral. Moreover, even if $x_0 \in \Sigma$, it is unlikely that $x_k = T_\epsilon^k(x)$ will ever come back to Σ (periodic points of T_ϵ are obvious exceptions) so the direct implementation of the Poincaré section is not possible. In order to visualise a trajectory $x_k = T_\epsilon^k(x_0)$ we implement the procedure explained in Section 3.2. The procedure consists in finding a subsequence k_j such that the trajectory jumps over Σ between x_{k_j} and x_{k_j+1}. We note that Σ does not divide the cylinder M into two subsets globally but, since the map T_ϵ is near identity, we can check this condition locally. Since Σ is defined by the equality $\psi_1 = \psi_2$, we look for k_j such that $(\psi_1^{k_j} - \psi_2^{k_j})(\psi_1^{k_j+1} - \psi_2^{k_j+1}) < 0$, where $x_k = (\psi_1^k, \psi_2^k, J_1^k, J_2^k)$ denotes the k-th iterate of $x_0 \in \mathbb{T}^2 \times \mathbb{R}^2$. Then a point $y_{k_j} \in \Sigma$ is defined by projecting x_{k_j} to Σ along the interpolating vector field X_n as defined by the equation (3.4).

Since the section Σ is three dimensional, the sequence y_{k_j} can be plotted and used to visually inspect the behaviour of the trajectory x_k.

On a moderate time scale, a further reduction of the dimension can be achieved by noting that h_n (defined by the equation (3.2)) is an adiabatic invariant of the map, so the trajectory x_k stays in a small neighbourhood of the set $M_E^n = \{x : h_n(x, \epsilon) = E\}$ where $E = h_n(x_0, \epsilon)$. Since M_E^n is close to M_E^0 and the latter is nicely described by the coordinates (ψ, ϕ), we can project the points y_{k_j} on the torus of coordinates (ψ, ϕ). In this way a trajectory of a 4-dimensional map is represented by a sequence of points on a two dimensional torus.

We remark that this procedure relies on the closeness of the map to the identity. Similar to the standard map, acceptable values of ϵ depend on the values of the variables J_1 and J_2. In our numerical experiments we use $|\epsilon| \leq 0.5$, so in practical terms the parameter does not need to be very small.

Visualization of the dynamics of T_ϵ

Examples of visualization of dynamics for T_ϵ are shown on Fig. 1 and 10. Some comments concerning the implementation can help the reader. First, the computation of the points y_{k_j} on Σ requires integration of X_n which is performed using a RK78 method that only requires evaluating the vector field. The time t_k in (3.4) is then computed using the Newton method in a way similar to [13].

Second, to show different trajectories on a single 2-dimensional torus we select initial conditions on $\Sigma_E^n = \Sigma \cap M_E^n$ for a fixed E. To find initial conditions with the same value of E, we use the following procedure: we select values of $\psi = 0, 1, 2, 3$ and, for each value, we compute a point $p = (\psi, \psi, 0, J_2^0)$, with $J_2^0 > 0$, such that $h_n(p, \epsilon) = E$ (using a bisection method with respect to J_2 to get a zero of $h_n(p, \epsilon) - E$). Since ∇h_n is orthogonal to the vector $(0, 0, -\partial h_n/\partial J_2, \partial h_n/\partial J_1)$, we numerically integrate the auxiliary vector field

$$\dot{J}_1 = -\frac{\partial h_n}{\partial J_2}\,, \qquad \dot{J}_2 = \frac{\partial h_n}{\partial J_1}\,, \tag{3.9}$$

with initial condition $(J_1(0), J_2(0)) = (0, J_2)$ (using a RK78 method). One obtains points $x_{0,i} = (\psi, \psi, J_1(t_i), J_2(t_i)) \in \Sigma_E^n$ for a sequence of t_i provided by the integration method. Finally, we use $x_{0,i}$ as initial conditions for the map T_ϵ.

Fig. 10 shows 500 projected iterates y_{k_j}, as defined by (3.4), obtained from the iterates x_{k_j} under the map T_ϵ for each of around 400 different initial conditions. The parameters of the map are defined by (3.7) and $\epsilon = 0.2$. The hyperbolic-hyperbolic fixed point p_4 is used as a base point x_b in the definition of the adiabatic invariant and the initial conditions are chosen on M_E^n with $n = 10$ and $E = 1$. We see that all points are located near a 2-dimensional torus embedded in the 3-dimensional surface Σ. The projection of the trajectories onto the coordinates (ψ, ϕ) resembles the dynamics of an area-preserving map.

Fig. 11(a) shows iterates of the point $(\psi_1, \psi_2, J_1, J_2) = (3, 3, -1.043523, 1.385456)$ that belongs to Σ_E^n with $E = 1$. This is one of the chaotic orbits which can be seen in Fig. 10. Fig. 11(b) shows a plot of the adiabatic invariant as a function of time along this orbit. For better visualization we show the value of the adiabatic invariant for one out of every 250 consecutive iterates of the point under T_ϵ. Some important observations follow from this plot:

- The orbit we study apparently belongs to a chaotic zone and is not located on a KAM torus.
- The adiabatic invariant is preserved (meaning that the range of oscillations remains unchanged) up to, at least, 10^6 iterates. Fig. 11(c) shows that this behaviour continues

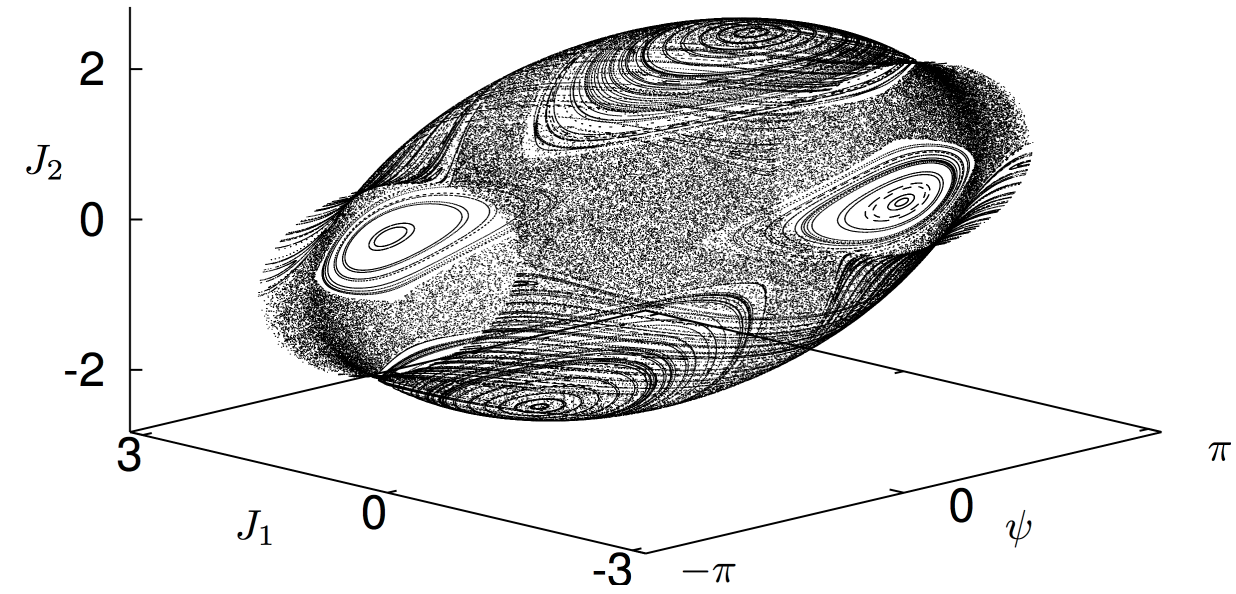

(a)

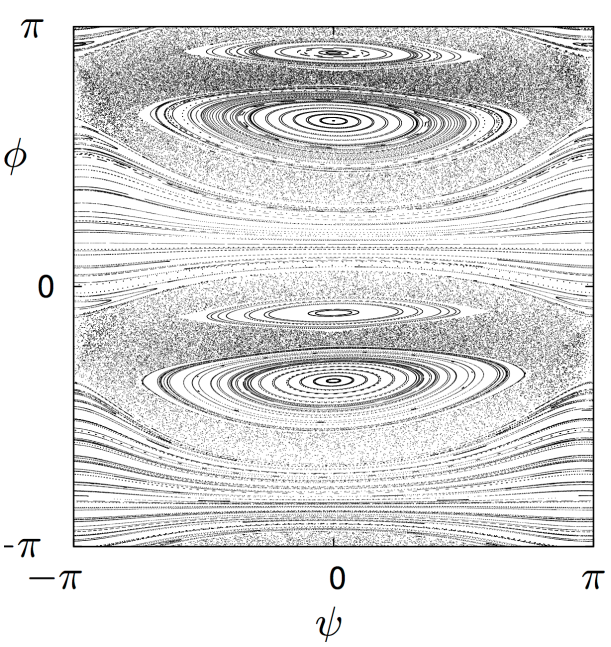

(b)

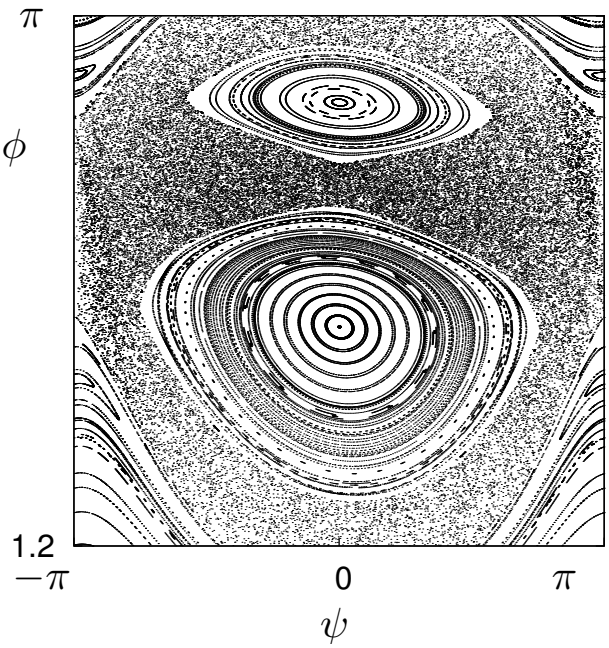

(c)

Figure 10: Trajectories of T_ϵ with the parameters defined by (3.7) and $\epsilon = 0.2$, $E = 1$, $n = 10$. (a) 500 projections y_{k_j} are plotted for each of 400 initial conditions taken on $\Sigma \cap M_E^n$, (b) projection of the points of (a) onto the torus with coordinates (ψ, ϕ), where $\phi = \arg(J_1 + iJ_2) \in (-\pi, \pi]$, (c) is a magnification from (b).

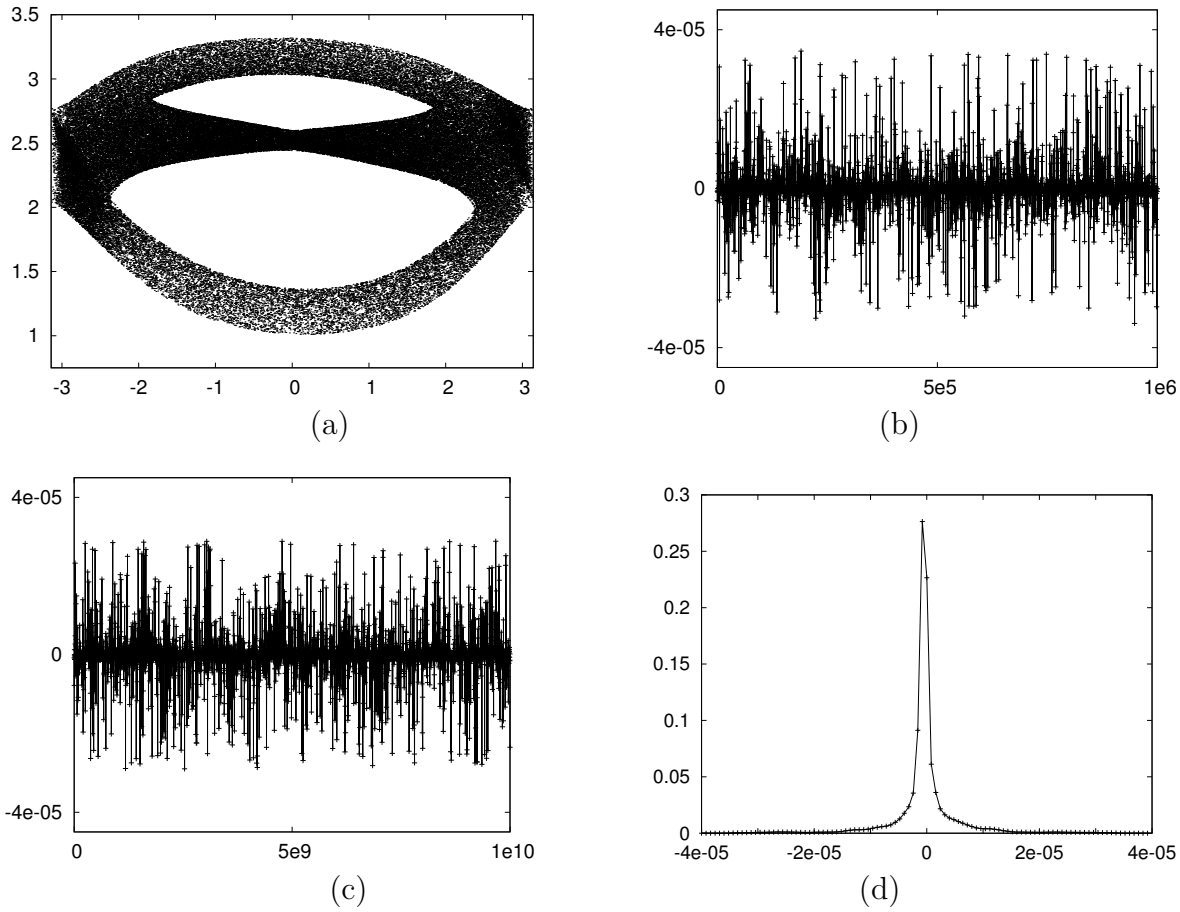

Figure 11: A single trajectory of the map T_ϵ with $\epsilon = 0.2$ for the initial point located at $(3, 3, -1.043523, 1.385456)$. (a) Points on the Poincaré section are represented using coordinates ψ_1 $(= \psi_2)$ and $\phi = \arg(J_1 + iJ_2) \in (-\pi, \pi]$; we show only one out of every ten consecutive points on the Poincaré section. (b) The adiabatic invariant h_n as a function of time (we show one point out of every 250 iterates). (c) The same as in (b) but up to 10^{10} iterates instead (we show one point out of every 250×10^4 iterates). (d) A histogram which illustrates the distribution of the adiabatic invariant for the Poincaré iterates up to $t = 10^6$. A bin size of 8×10^{-7} has been used to obtain the distribution.

at least for 10^{10} iterates of T_ϵ. The dynamical interpretation of such preservation is clear: our numerical method has detected the slowest variable of the system which evolves on a very long time scale. We note that in this example one expects to see an (Arnold like) diffusion process and, in particular, the slow variable requires exponentially long (with respect to ϵ^{-1}) time to be changed by order one. Our method is able to detect such a slow variable in a simple and efficient way.

- There is no systematic drift of the adiabatic invariant. Its values are distributed in a Gaussian-like way around the initial value (see Fig. 11(d)). We remark that, for T_ϵ and the chosen parameters, there is numerical evidence supporting that the detection of the expected drift in the adiabatic invariant due to the Arnold diffusion process requires a much longer time scaling.

A final illustration of the amount of details one can visualize with this methodology is presented in Fig. 1. There we show a plot similar to the one in Fig. 10 but for $\epsilon = 0.35$ and $E = 4$. As before, we take the hyperbolic-hyperbolic fixed point p_4 as a base point to define the adiabatic invariant. The interpolating vector field is constructed with $n = 10$. One can clearly recognize the typical structures that show up in a phase space of an area-preserving map: islands of stability (including secondary islands and satellites in the chaotic zone), invariant curves and chaotic zones. Yet this is not a 2-dimensional map: we are just plotting a suitable projection (along the solutions of the interpolating vector field) of the iterates of the 4-dimensional map!

4 Conclusions

It has been known for a long time that the combination of a time-periodic suspension with the averaging method can be used to construct an autonomous vector field which approximately interpolates a near identity map F_ϵ. In this paper we show that an interpolating vector field can be constructed directly from iterates of the map: $\epsilon X_n = \sum_{k=-n}^{n} p_{nk} F_\epsilon^k$ where the weights p_{nk} are constant and independent of the map (see equation (1.3)). In this way the averaging procedure is reduced to computing a weighted sum of the iterates of the map. Similarly to the classical averaging procedure, the parameter n controls the order of the interpolation error and by taking $n \sim \epsilon^{-1}$ the error can be made exponentially small.

The simplicity of the expression for the interpolating vector field X_n makes it a useful tool in numerical studies of the dynamics. In particular, projections along X_n can be used to define a "Poincaré section" for the map which help to visualise dynamics by reducing dimension of the pictures.

In the case of a symplectic F_ϵ the interpolating vector field X_n is close to a Hamiltonian one and can be used to construct an adiabatic invariant of the map. We use the adiabatic invariant to achieve further reduction in the dimension and obtain two-dimensional pictures showing details of the dynamics for a four-dimensional Froeschlé-like map.

Our method does not require the map to be near the identity globally: it is sufficient to know that a certain iterate of a map is near identity on a subset of the phase space.

We are confident that the interpolating vector fields can be useful in other analytical and numerical studies. In particular, we used them in a quantitative study of the Arnold diffusion and we will report on the corresponding results elsewhere. We expect that the projection along an interpolating vector field can be used in combination with the method of slices. Finally, the interpolating vector fields are potentially applicable to analysis of time series where the precise form of the map is not known.

5 Acknowledgments

AV has been supported by grants MTM2016-80117-P (MINECO/FEDER) (Spain) and 2014-SGR-1145 (Catalonia). VG's research was supported by EPRC (grant EP/J003948/1). The authors are grateful to Ernest Fontich and Carles Simó for useful discussions and remarks.

References

[1] Benettin, G.; Giorgilli, A.; *On the Hamiltonian interpolation of near-to-the identity symplectic mappings with application to symplectic integration algorithms*, Journal of Statistical Physics (1994) vol. 74, issue 5-6, pp 1117–1143.

[2] Bogoliubov, N. N.; Mitropolsky, Y. A.; *Asymptotic methods in the theory of non-linear oscillations*. Gordon and Breach Science Publishers, New York 1961, 537 pp.

[3] Broer, H., Roussarie, R., and Simó, C.; *Invariant circles in the Bogdanov-Takens diffeomorphisms.* Ergod. Th. and Dynam. Sys., 16:1147 – 1172, 1996.

[4] Chirikov, B.V.; *A universal instability of many-dimensional oscillator system*. Phys. Rep., 52 (1979), 264–379.

[5] Dullin, H.R.; Meiss, J.D.; *Quadratic Volume-Preserving Maps: Invariant Circles and Bifurcations*. Siam J. Applied Dynamical Systems 8(1), 76–128.

[6] Efthymiopoulos, C.; Harsoula, M.; *The speed of Arnold diffusion*, Physica D vol. **251** issue 1 (2013) pp. 19–38.

[7] Gelfreich, V., *Numerics and exponential smallness*. In Handbook of dynamical systems, Vol. 2, 265–312, North-Holland, Amsterdam, 2002.

[8] Gelfreich, V., Simó, C., and Vieiro A.; *Dynamics of 4D symplectic maps near a double resonance*, Physica D vol. **243** issue 1 (2013) pp. 92–110.

[9] Kuksin, S.; Pöschel, J.; *On the inclusion of analytic symplectic maps in analytic Hamiltonian flows and its applications*. In Seminar on Dynamical Systems (St. Petersburg, 1991), 96–116, Progr. Nonlinear Differential Equations Appl., 12, Birkh auser, Basel, 1994.

[10] Neishtadt, A.I.; *The separation of motions in systems with rapidly rotating phase*, J.Appl. Math. Mech., 48 (1984), 133–139.

[11] Nekhoroshev N.N.; *An exponential estimate of the time of stability of nearly integrable Hamiltonian systems.* Russian Mathematical Surveys, 32(6) (1977) 1–65.

[12] Richter M.; Lange S.; Bcker A.; Ketzmerick R.; *Visualization and comparison of classical structures and quantum states of four-dimensional maps.* Phys. Rev. E 89(2) (2014) 022902

[13] Simó, C.; *On the Analytical and Numerical Approximation of Invariant Manifolds*, Les Méthodes Modernes de la Mecánique Céleste (Course given at Goutelas, France, 1989), D. Benest and C. Froeschlé (eds.), pp. 285–329, Editions Frontires, Paris, 1990.

[14] Simó, C.; *Analytic and numeric computations of exponentially small phenomena*, In K. Gröger B. Fiedler and J. Sprekels, editors, *Proceedings EQUADIFF 99, Berlin*, pages 967 – 976, 2000. World Scientific, Singapore.

[15] Stoer, J; Bulirsch, R.; *Introduction to Numerical Analysis.* Third edition. Texts in Applied Mathematics, 12. Springer-Verlag, New York, 2002. xvi+744 pp.

[16] Takens, F.; *Forced oscillations and bifurcations*, Applications of Global Analysis I. Communications of the Mathematical Institute Rijksuniversiteit Utrecht, 3, 1974.